Article

Epithelial IFNγ signalling and compartmentalized antigen presentation orchestrate gut immunity

https://doi.org/10.1038/s41586-023-06721-1

Received: 30 June 2022

Accepted: 6 October 2023

Published online: 22 November 2023

Check for updates

Ankit Malik[1]✉, Deepika Sharma[1], Raúl Aguirre-Gamboa[1], Shaina McGrath[1], Sarah Zabala[1], Christopher Weber[1,2] & Bana Jabri[1]✉

All nucleated cells express major histocompatibility complex I and interferon-γ (IFNγ) receptor[1], but an epithelial cell-specific function of IFNγ signalling or antigen presentation by means of major histocompatibility complex I has not been explored. We show here that on sensing IFNγ, colonic epithelial cells productively present pathogen and self-derived antigens to cognate intra-epithelial T cells, which are critically located at the epithelial barrier. Antigen presentation by the epithelial cells confers extracellular ATPase expression in cognate intra-epithelial T cells, which limits the accumulation of extracellular adenosine triphosphate and consequent activation of the NLRP3 inflammasome in tissue macrophages. By contrast, antigen presentation by the tissue macrophages alongside inflammasome-associated interleukin-1α and interleukin-1β production promotes a pathogenic transformation of $CD4^+$ T cells into granulocyte–macrophage colony-stimulating-factor (GM-CSF)-producing T cells in vivo, which promotes colitis and colorectal cancer. Taken together, our study unravels critical checkpoints requiring IFNγ sensing and antigen presentation by epithelial cells that control the development of pathogenic $CD4^+$ T cell responses in vivo.

Inflammatory bowel diseases (IBDs) affect more than five million individuals worldwide and constitute a significant expanding health problem[2,3]. The risk of developing colorectal cancer (CRC) is also increased by fourfold with the development of IBD, and CRC is a leading cause of cancer-related death in adults[4]. Intestinal epithelial cells (IECs) reside at the interface of the microbiota and the mucosal immune system, and IEC dysfunction is associated with the development of IBD and CRC[5–7]. However, the mechanisms by which IECs regulate pathogenic CD4 T cell responses and prevent IBD and CRC remain poorly understood.

IECs express interferon-γ receptors 1 and 2 (IFNγR1 and IFNγR2), which oligomerize and transphosphorylate on ligand binding, activating Janus-activated kinase 1 (JAK1) and JAK2. JAK1 and JAK2, in turn, phosphorylate IFNγR1, creating a docking site for the signal transducer and activator of transcription 1 (STAT1). JAK1/2-phosphorylated STAT1 homodimerizes and translocates to the nucleus to induce the expression of the transcription factor interferon-regulatory factor 1 (IRF1), which in turn promotes major histocompatibility complex (MHC) class I (MHCI) and II (MHCII) expression and antigen presentation[8,9]. The STAT1 cascade can also be activated by type I and type III interferons[8,10,11], but the relative contribution of different interferons to the epithelial STAT1 cascade is unknown. Single nucleotide polymorphisms (SNPs) in IFNγR1, IFNγR2 and downstream mediators JAK2, STAT1 and human leukocyte antigen-C are significantly associated with the development of IBD and CRC[12,13]. However, the function of IFNγ sensing or antigen presentation by means of MHCI by IECs in colitis or CRC is unknown.

Epithelial IFNγ signalling is protective in colitis

To determine whether epithelial IFNγ signalling is modulated in IECs during infectious colitis, we infected wild-type (WT) C57BL/6J mice with *Citrobacter rodentium*, a physiologically relevant mouse model of acute colitis that mirrors human infection with enteropathogenic and enterohaemorrhagic *Escherichia coli*[14,15]. IFNγ transcript in the colon increased on day 6, peaked on day 12, and returned to baseline level by day 21 post-infection (p.i.), mirroring the colonization kinetics of *C. rodentium* (Extended Data Fig. 1a,b). Activation of STAT1 (pTyr701) (Extended Data Fig. 1c,d) and increase in IRF1 expression (Extended Data Fig. 1e) in IECs correlated with the kinetics of the IFNγ expression, peaking at day 12 p.i. To evaluate the role of epithelial IFNγ signalling in colitis, we generated IEC-specific IFNγR1-deficient mice and orally infected littermate $Ifngr^{fl/fl}$ and $Ifngr^{fl/fl}Vil^{Cre}$ (referred to as $Ifngr^{\Delta IEC}$) mice with *C. rodentium*. The absence of IFNγ signalling in IECs did not affect pathogen colonization or colon length early during infection (day 6) (Fig. 1a,b). However, at day 12 p.i., the peak of acute colitis in this model[16], $Ifngr^{\Delta IEC}$ mice had significantly more severe colitis as assessed by a shorter colon (Fig. 1b) and increased neutrophil infiltration in the

[1]Department of Medicine, Committee on Immunology, Department of Pediatrics, Department of Pathology, University of Chicago, Chicago, IL, USA. [2]Department of Pathology, Department of Medicine, University of Chicago, Chicago, IL, USA. ✉e-mail: malikank@uchicago.edu; bjabri@bsd.uchicago.edu

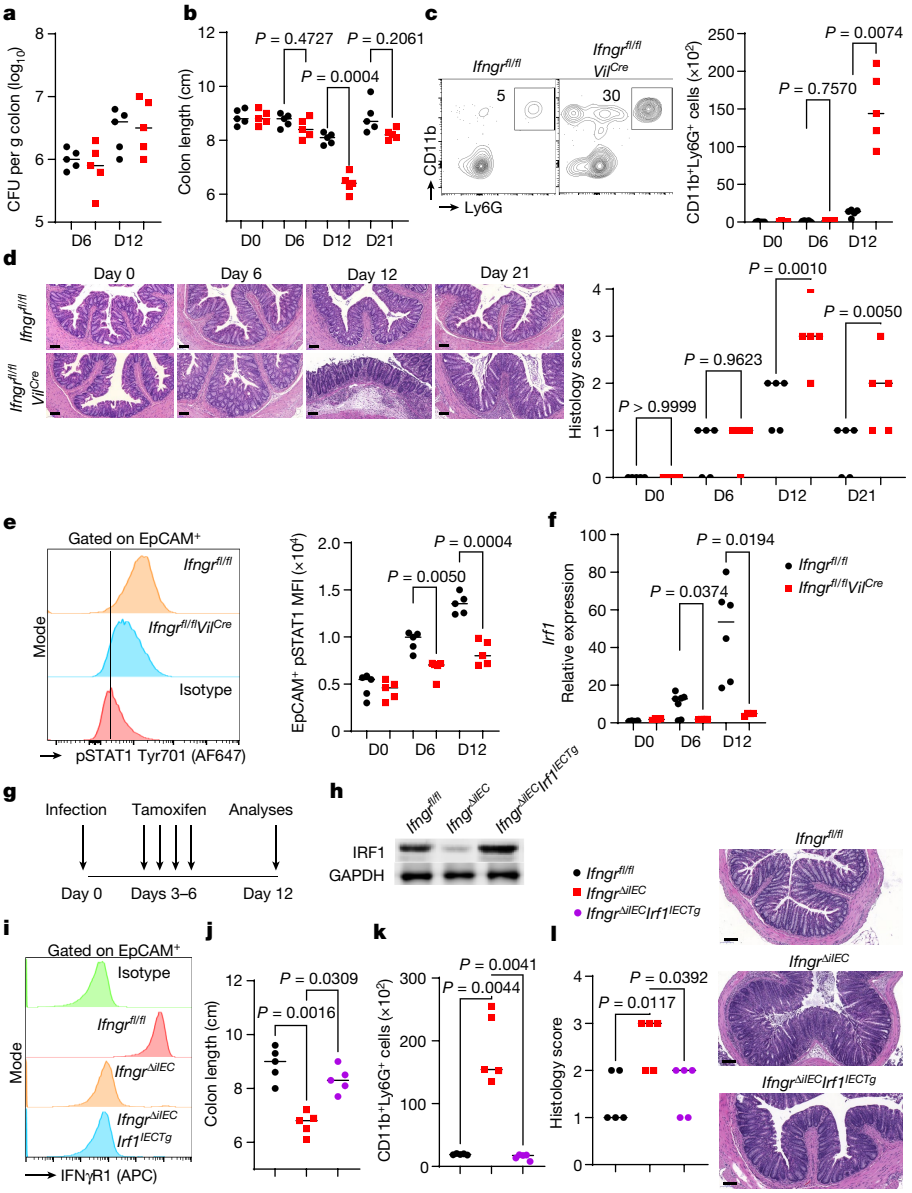

Fig. 1 | Epithelial sensing of IFNγ protects from colitis by means of upregulation of IRF1. *Ifngr1*$^{fl/fl}$ and *Ifngr1*$^{fl/fl}$*Vil*^{Cre} mice were infected with *C. rodentium*. **a**–**c**, *Citrobacter* colonization in colon (**a**), colon length (**b**) and enumeration (**c**) of the CD11b$^+$Ly6G$^+$ cells in the epithelium at the indicated day p.i. and representative flow cytometry plot gated on CD45$^+$Lin$^-$ (EpCAM, Ter119, CD19, TCR$^-$) cells at day 12 ($n = 5$ per group). **d**, Representative pictures of H&E-stained colon sections at ×100 magnification and histology scores. **e**, STAT1 pTyr701 analyses in EpCAM$^+$ cells by flow cytometry and representative flow cytometry plot gated on EpCAM$^+$CD45$^-$ cells at day 12 ($n = 5$ per group). **f**, Quantification of *Irf1* transcript in purified EpCAM$^+$ IECs ($n = 4$ *Ifngr1*$^{fl/fl}$ and $n = 6$ *Ifngr1*$^{fl/fl}$*Vil*^{Cre}). **g**, *Ifngr1*$^{fl/fl}$, *Ifngr1*$^{fl/fl}$*Vil*^{CreERT2} and *Ifngr1*$^{fl/fl}$*Vil*^{CreERT2}*R26*^{LSLIrf1} mice were infected with *C. rodentium* on day 0, injected with tamoxifen at days 3–6 p.i., and analysed on day 12 ($n = 5$ per group). **h**, Immunoblotting for IRF1 in the purified IECs (representative of two independent experiments). **i**, Flow cytometric analyses of IFNγR1 in IECs. **j**, Colon length. **k**, Enumeration of the proportion of CD11b$^+$Ly6G$^+$ cells in CD45$^+$Lin$^-$ (EpCAM, Ter119, CD19, TCR$^-$) cells in the epithelial compartment. **l**, Histology score and representative H&E-stained colon section at ×100 magnification ($n = 5$ per group). The horizontal bar represents the median, and each symbol and lane in the immunoblot represents an individual mouse. Data were analysed by analysis of variance (ANOVA) tests (**a**–**f**,**k**) followed by the Dunnet's or Sidak post hoc test or Kruskal–Walis test followed by Dunn's post-test (**j**,**l**). Scale bar, 100 µm. CFU, colony-forming unit; MFI, median fluorescence intensity.

epithelium (Fig. 1c). Furthermore, histological analysis revealed an increase in the infiltration of mono- and polymorphonuclear (PMN) cells and goblet cell dysplasia in the colons of *Ifngr*$^{\Delta IEC}$ mice (Fig. 1d). *C. rodentium* infection was cleared to undetectable levels in both groups by day 21. However, colon histology was worse in *Ifngr*$^{\Delta IEC}$ mice at day 21, indicating delayed resolution of inflammation in *Ifngr*$^{\Delta IEC}$ mice (Fig. 1d). Activation of STAT1 (Fig. 1e) and upregulation of IRF1 (Fig. 1f) were largely absent in the IFNγR-deficient IECs, demonstrating that IFNγ is the main driver of the STAT1–IRF1 cascade in IECs during colitis.

To determine whether the lack of IRF1 upregulation in IECs contributed to the severe colitis observed in *Ifngr*$^{\Delta IEC}$ mice, we generated cell-type-specific IRF1 transgenic mice *R26*^{LSLIrf1} using CRISPR–Cas9 mediated gene editing and crossed them to *Ifngr*$^{fl/fl}$*Vil*^{CreERT2} mice (*Ifngr*$^{\Delta iIEC}$*Irf1*^{IECTg}). On tamoxifen treatment early during infection (days 3–6, Fig. 1g), transgenic expression of IRF1 in the *Ifngr*$^{\Delta iIEC}$*Irf1*^{IECTg} IECs protected against colitis when compared to the littermate *Ifngr*$^{\Delta iIEC}$ mice, despite the absence of IFNγR1 expression in IECs (Fig. 1h–l). Taken together, these data demonstrate that the IFNγR–IRF1 pathway plays

a significant role in protection against *C. rodentium*-induced colitis independently of pathogen colonization.

Epithelial IFNγ signalling restricts colitogenic T cells

C. rodentium is an epithelium-attaching pathogen that induces a $CD4^+$ T cell response[14,17,18]. To determine the immunological basis of protection from colitis conferred by IFNγ signalling in IECs, we analysed the intra-epithelial T (IE-T) cell response in the colon at day 0 (baseline), day 6 (predisease), and day 12 p.i. We observed a time-dependent increase in the number of T cell receptor (TCR)$\alpha\beta^+CD4^+$ IE-T cells during infection (Extended Data Fig. 2a). Consistent with increased colitis, the number and proportion of $CD4^+$ IE-T cells were higher in the colons of $Ifngr^{\Delta IEC}$ mice when compared to $Ifngr^{fl/fl}$ colons at day 12 p.i. (Extended Data Fig. 2a,b). Furthermore, the $CD4^+$ IE-T cells of the $Ifngr^{\Delta IEC}$ mice produced more IL-17A, IFNγ and granulocyte–macrophage colony-stimulating factor (GM-CSF) at day 12 p.i. than the $CD4^+$ IE-T cells from the $Ifngr^{fl/fl}$ colons (Extended Data Fig. 2c–f). The increase in IL-17A production was driven by the $GM\text{-}CSF^+CD4^+$ T cell subset, as the proportion of $GM\text{-}CSF^-IL\text{-}17A^+$ cells was unchanged during the infection (Extended Data Fig. 2c–e). In contrast to the increase in $GM\text{-}CSF^+CD4^+$ T cells, the proportion of $CD4^+FoxP3^+$ regulatory T cells and the numbers of $CD4^+CD8\alpha\alpha^+$ (double positive), $CD4^-CD8\alpha^-$ (double negative) or $TCR\gamma\delta^+$ IE-T cells and ($CD90^{hi}TCR\beta^-TCR\gamma\delta^-$) innate lymphoid cells (ILCs) were similar between the colons of $Ifngr^{fl/fl}$ and $Ifngr^{\Delta IEC}$ mice throughout the infection (Extended Data Fig. 2g–k). $CD11b^+F480^+$ macrophages were increased at day 12 p.i. in the colons of $Ifngr^{\Delta IEC}$ mice (Extended Data Fig. 2l), and although a proportion of ILCs produced GM-CSF, a robust increase in GM-CSF production was observed mainly in the $CD4^+$ T cells (Extended Data Fig. 2m). Furthermore, per-cell production (median fluorescence intensity (MFI)) of GM-CSF was significantly higher in the $CD4^+$ T cells than ILCs (Extended Data Fig. 2n), and $CD4^+$ T cells were the predominant source of IFNγ, IL-17A and GM-CSF (Extended Data Fig. 2o) in the colons of $Ifngr^{\Delta IEC}$ mice.

To test whether the $CD4^+$ T cell responses were specific to bacterial or epithelial-derived antigens during *Citrobacter* infection, we generated a strain of *C. rodentium* that expresses the model antigen ovalbumin (ova) from its chromosome ($Citro^{Ova}$) (Fig. 2a and Extended Data Fig. 3a–d) and cell-type-specific ova transgenic mouse model ($R26^{LSLOva}$) using CRISPR–Cas9 mediated gene editing (Fig. 2d), respectively. To assess the *C. rodentium*-specific T cell response, we infected littermate $Ifngr^{fl/fl}$ and $Ifngr^{\Delta IEC}$ mice with $Citro^{ova}$. To assess epithelial-specific T cell responses, we crossed $R26^{LSLOva}$ mice to $Ifngr^{fl/fl}Vil^{CreERT2}$ mice to generate a mouse model that simultaneously lacks IFNγR and expresses ova from IECs upon tamoxifen administration ($Ifngr^{fl/fl}Vil^{creERT2}Ova^{Tg}$). Littermate control $Ifngr^{fl/fl}Vil^{creERT2}R26^{LSLOva}$ and $Ifngr^{fl/+}Vil^{creERT2}R26^{LSLOva}$ mice were infected with WT *Citrobacter* and administered tamoxifen on days 3–6 p.i. to assess the response to an epithelial antigen. Absence of IFNγR on IECs led to increased recruitment of both pathogen- and epithelial-specific $CD4^+$ T cell responses, as assessed by ova–tetramer reactivity at day 12 p.i. (Fig. 2b,e). Pathogen- and IEC-specific $CD4^+$ IE-T cells also had a higher proportion of $GM\text{-}CSF^+IL\text{-}17A^-$, $GM\text{-}CSF^+IL\text{-}17A^+$ and $IFN\gamma^+$ subsets in $Ifngr^{\Delta IEC}$ mice than the respective littermate control mice, and $GM\text{-}CSF^+$ cells were also $IFN\gamma^+$ (Fig. 2c,f, and Extended Data Fig. 3e,f). The pathogen- and IEC-specific $CD4^+$ IE-T cells were newly infiltrating and not resident T cells, as they expressed the gut homing receptor α4β7, which is downregulated on acquisition of tissue residency[19], and had low expression of the tissue residency marker[19] CD103 (Extended Data Fig. 3g). Furthermore, the exacerbated polyclonal and pathogen-specific $CD4^+GM\text{-}CSF^+$ IE-T cell responses observed in the colons of $Ifngr1^{\Delta IEC}$ mice were prevented on transgenic expression of IRF1 in IECs without affecting the burden of *C. rodentium* in the colon (Extended Data Fig. 3h–k).

GM-CSF is being increasingly incriminated in complex immune disorders, including colitis[20–24], and the production of GM-CSF was higher in the $CD4^+$ IE-T cells obtained from $Ifngr^{\Delta IEC}$ mice. To determine whether the $CD4^+$ T cells producing GM-CSF were driving the exacerbated colitis in $Ifngr^{\Delta IEC}$ mice, we partially depleted $CD4^+$ T cells or neutralized GM-CSF starting at day 7 p.i. In accordance with the hypothesis, depleting $CD4^+$ T cells decreased GM-CSF and blocking GM-CSF or depleting $CD4^+$ T cells mitigated colitis in $Ifngr^{\Delta IEC}$ mice (Fig. 2h,i and Extended Data Fig. 3l). Taken together, our results reveal that the absence of IFNγ sensing by IECs leads to increased pathogen and epithelial-specific $CD4^+GM\text{-}CSF^+$ T cell response, and IFNγ-induced IRF1 expression in IECs is sufficient to restrain these colitogenic T cells.

Macrophage antigen presentation promotes colitogenic T cells

GM-CSF production from $CD4^+$ T cells is induced by IL-1β (refs. 20,25,26), and the secretion of bioactive IL-1β depends on inflammasome activation[27,28]. IL-1α is another IL-1R ligand that is released from cells during pyroptosis and retains bioactivity with or without processing by caspase-1 (ref. 29). However, the checkpoints and cellular circuits that regulate the development of pathogenic $CD4^+GM\text{-}CSF^+$ T cell responses in vivo remain poorly understood. We first analysed IL-1β secretion and inflammasome activation in the colons of $Ifngr^{\Delta IEC}$ mice on *C. rodentium* infection and found that $Ifngr^{\Delta IEC}$ mice exhibited increased IL-1β (and GM-CSF) secretion by colonic explants (Extended Data Fig. 4a,b) and cleaved caspase-1 in colonic lysates compared to littermate controls at day 12 p.i. (Extended Data Fig. 4c). Because extracellular adenosine triphosphate (ATP) is a damage-associated molecular pattern and a potent inducer of the NLRP3 inflammasome[30–32], we analysed ATP secretion by colonic explants and found that it was increased during infection and significantly higher in $Ifngr^{\Delta IEC}$ mice at day 12 p.i. (Fig. 3a). To directly test whether the ATP–NLRP3–IL-1β axis drives severe colitis in *C. rodentium*-infected $Ifngr^{\Delta IEC}$ mice, we assessed the sufficiency and requirement of this axis in the induction of the colitogenic GM-CSF response. αβ-ATP is a non-hydrolysable form of ATP that cannot be used as an energy source by cells but can activate the P2X7 receptor[33]. Administration of αβ-ATP to $Ifngr^{fl/fl}$ control mice during *C. rodentium* infection was sufficient to increase caspase-1 cleavage, IL-1β and IL-1α secretion, and GM-CSF production (Fig. 3b–d and Extended Data Fig. 4d) in the colon, which was associated with increased colitis (Fig. 3e,f and Extended Data Fig. 4e). Conversely, a protective effect was observed when $Ifngr^{\Delta IEC}$ mice were treated with exogenous ATPase (apyrase), a clinical dose of the specific NLRP3 inhibitor MCC950 or an IL-1R antagonist starting at day 7 p.i. (Fig. 3b–f and Extended Data Fig. 4e,f) without affecting the burden of *C. rodentium* in the colon (Extended Data Fig. 4g). Macrophages were a significant source of the inflammasome-associated IL-1β response as depletion of macrophages by CSF-1R blockade significantly reduced the amount of IL-1β and GM-CSF secretion from the $Ifngr^{\Delta IEC}$ colon explants (Extended Data Fig. 4h,i), concomitant with reduced numbers of $CD4^+$ IE-T cells, production of GM-CSF and colon shortening (Extended Data Fig. 4j,k).

While IL-1β and other innate factors influence the differentiation of T cells, TCR–MHC interaction is also required for the survival and proliferation of $CD4^+$ T cells. During colitis, $CX3CR1^+$ antigen-presenting cells (APCs) made up a bulk of the $MHCII^+$ cells in the immune $CD45^+$ compartment (Fig. 3f). We therefore determined the function of MHCII expression by $CX3CR1^+$ APCs in the pathogenic transformation of $CD4^+$ IE-T cells during colitis. To this end, we crossed *CX3CR1-creERT2* (ref. 34) mice to $H2ab^{fl/fl}$ mice to generate a model of inducible MHCII deletion in $CX3CR1^+$ cells upon tamoxifen treatment ($H2ab^{\Delta iCX3CR1}$). Furthermore, by transferring bone marrow from $H2ab^{fl/fl}$ or $H2ab^{\Delta iCX3CR1}$ mice into lethally irradiated $Ifngr^{fl/fl}$ or $Ifngr^{\Delta iIEC}$ mice, we generated mouse models wherein we can simultaneously delete IFNγR in IECs and MHCII in $CX3CR1^+$ cells (experimental strategy in Fig. 3g). This model allows for efficient deletion of MHCII in macrophages, but not

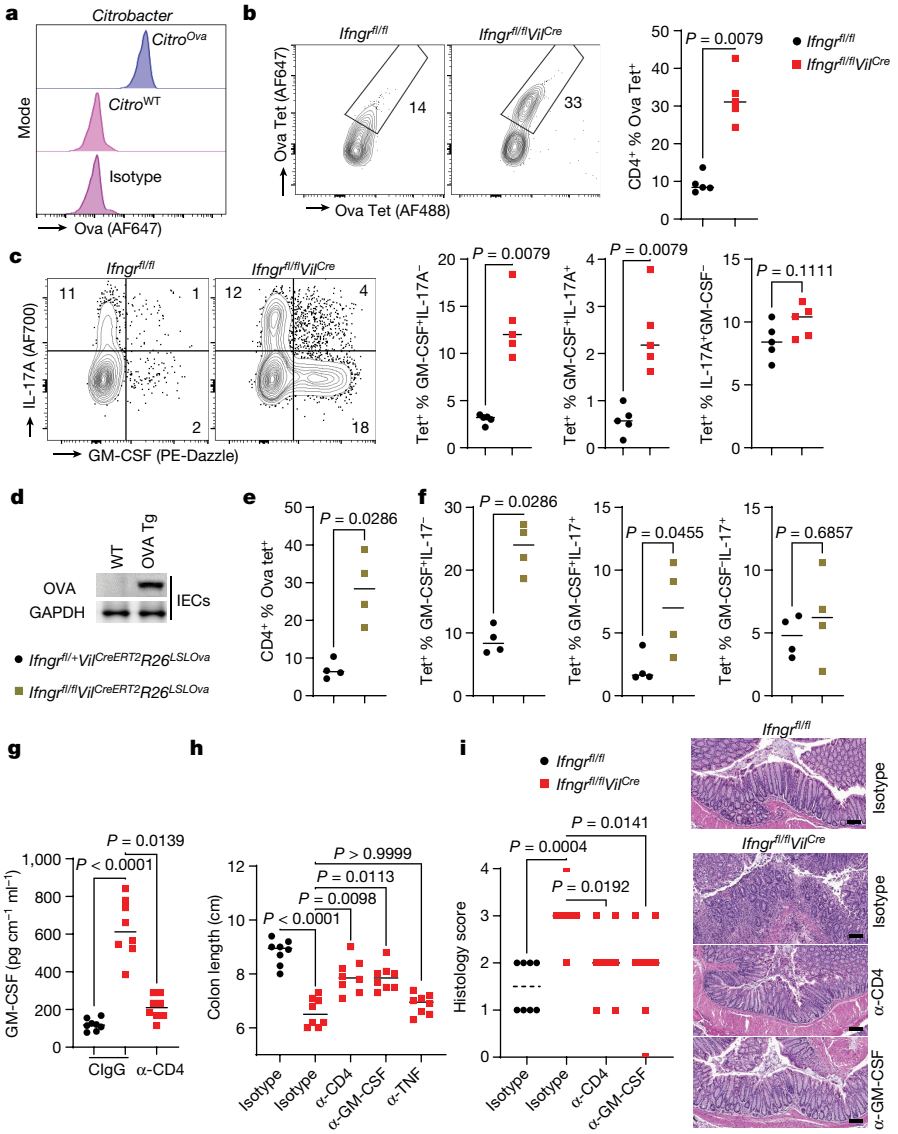

Fig. 2 | Epithelial sensing of IFNγ restrains pathogenic CD4 GM-CSF response. a, Flow cytometric analysis of ova expression by *Citrobacter*. **b**, Representative flow cytometry plot and enumeration of ova-specific CD4$^+$ IE-T cells. **c**, Intracellular staining in ova-specific CD4$^+$ IE-T cells obtained from the colons of *Ifngr1*$^{fl/fl}$ and *Ifngr1*$^{fl/fl}$*Vil*^{Cre} mice at day 12 p.i. with the ova$^+$ *Citrobacter* ($n = 5$ per group). **d**, *R26*^{LSLOva} and *Vil*^{CreERT2}*R26*^{LSLOva} mice were injected with tamoxifen for four consecutive days, and purified IECs were analysed for the expression of ova by immunoblotting ($n = 4$ per group). **e**,**f**, *Ifngr1*$^{fl/+}$*Vil*^{CreERT2}*R26*^{LSLOva} and *Ifngr1*$^{fl/fl}$*Vil*^{CreERT2}*R26*^{LSLOva} mice were infected with *C. rodentium* on day 0, injected with tamoxifen on days 3–6 p.i. and sacrificed on day 12. Enumeration of ova-specific CD4$^+$ IE-T cells (**e**) and intracellular staining in them (**f**) ($n = 4$ per group). Intracellular staining for IL-17A, IFNγ and GM-CSF was performed after brief restimulation. **g**–**i**, *Ifngr1*$^{fl/fl}$ and *Ifngr1*$^{fl/fl}$*Vil*^{Cre} mice were infected with *Citrobacter*; treated with anti-CD4, anti-GM-CSF or anti-TNF antibodies every two days starting at day 7; and sacrificed on day 12 p.i. ($n = 8$ per group) GM-CSF in colon explant (**g**), colon length (**h**) and histology score and representative H&E-stained colon section at ×100 magnification (**i**). Each symbol represents an individual mouse, and the bar indicates the median. Data were analysed by Mann–Whitney U test (two-sided; **b**,**c**,**e**,**f**) or Kruskal–Wallis test followed by Dunn's post-test (**g**–**i**). Scale bar, 100 µm.

cDC2s (F4/80$^-$Ly6C/Ly6G$^-$CD11c$^+$CD172a$^+$) (Extended Data Fig. 5a). And after infection with *C. rodentium*, *H2ab*$^{\Delta iCX3CR1}$»*Ifngr*$^{\Delta iIEC}$ chimeric mice had a significantly blunted CD4$^+$ GM-CSF$^+$IL-17A$^-$ and GM-CSF$^+$IL-17A$^+$ response (Fig. 3h and Extended Data Fig. 5b) and colon-length shortening (Fig. 3i) compared to *H2ab*$^{fl/fl}$»*Ifngr*$^{\Delta iIEC}$ mice. Further, CX3CR1$^+$ APCs seem to be involved in the priming of T_H1 cells as the acquisition of T-bet in adoptively transferred Rag-OTII cells in mesenteric lymph nodes (MLNs) was decreased on MHCII deletion in CX3CR1$^+$ cells (Extended Data Fig. 5c). Overall, these data demonstrate that MHCII-mediated antigen presentation by CX3CR1$^+$ APCs mediates the pathogenic transformation of CD4$^+$ IE-T cells and exacerbated colitis when IECs lack IFNγR.

IEC antigen presentation promotes eATPase in T cells

Although ATP is present at high concentrations intracellularly (up to 100 µM), its extracellular levels are tightly controlled by extracellular ATPases (eATPases) such as ENTPD1 (also known as CD39) and ENTPD5 (refs. 35–37). The expression of *Entpd1* and *Entpd5* was increased in the colons of littermate control mice during *C. rodentium* infection but attenuated in the colons of *Ifngr*$^{\Delta IEC}$ mice at days 6 and 12 p.i. (Extended Data Fig. 6a,b). To assess the cellular source of CD39, we used unbiased gating and found that CD8αβ$^+$ and CD4$^+$ IE-T cells were the principal sources of CD39 during *C. rodentium* infection (Extended Data Fig. 6c). IFNγ signalling in IECs controlled the overall number of CD39$^+$ IE-T cells

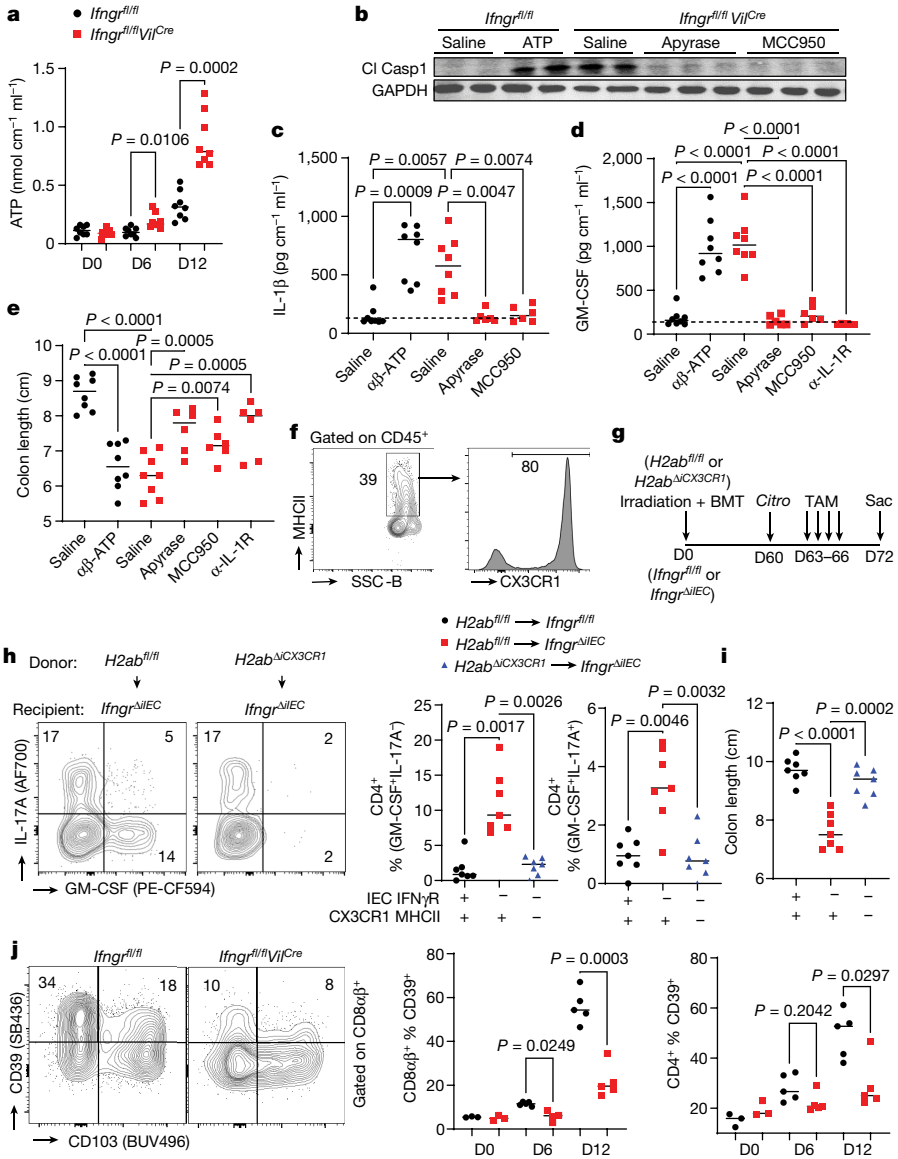

Fig. 3 | Epithelial sensing of IFNγ promotes eATPase expression in IE-T cells to restrain the colitogenic NLRP3 inflammasome. *Ifngr1*$^{fl/fl}$ and *Ifngr1*$^{fl/fl}$*Vil*^{Cre} mice were infected with *C. rodentium*. **a**, Quantification of ATP secreted by the colon explants ($n = 8$ per group). *Ifngr1*$^{fl/fl}$ and *Ifngr1*$^{fl/fl}$*Vil*^{Cre} mice were infected with *Citrobacter* and treated with an isotype ($n = 8$), αβ-ATP ($n = 8$), apyrase ($n = 6$), MCC950 ($n = 6$) or anti-IL-1R ($n = 6$) starting on day 7 and sacrificed on day 12 p.i. **b**, Immunoblotting for cleaved caspase-1 in the colon lysates. **c**,**d**, ELISA for IL-1β (**c**) and GM-CSF (**d**) in the colon explant supernatants. **e**, Colon length. **f**, Flow cytometric analysis MHCII expression by CX3CR1$^+$ cells in WT colon at day 12 p.i. **g**, Experimental strategy. **h**, GM-CSF and IL-17A production in CD4$^+$ IE-T cells. **i**, Colon length at day 72 ($n = 7$ per group). **j**, CD39 expression in CD8αβ$^+$ and CD4$^+$ IE-T cells at indicated days p.i. ($n = 3$ for day 0 and $n = 5$ for rest of the groups). Each symbol represents an individual mouse, and the bar indicates the median. Data were analysed by ANOVA tests followed by the Dunnet's post hoc test. *P* value is two-sided. α, anti.

(Extended Data Fig. 6d,e), and the expression of CD39 and *Entpd5* in both CD8αβ$^+$ and CD4$^+$ IE-T cells but not in IECs (Fig. 3j and Extended Data Fig. 6f,g). CD39 was upregulated in both tissue-resident CD103$^+$ and de novo recruited CD103$^-$ IE-T cells (Fig. 3j and Extended Data Fig. 6h) and involved pathogen and IEC-specific IE-T cells (Extended Data Fig. 6i). Among CD4$^+$ IE-T cells, distinct subsets expressed CD39 and GM-CSF (Extended Data Fig. 6j), indicating discrete induction mechanisms for these two T cell subsets. Because the decrease in absolute numbers of CD39$^+$ cells involved mostly the CD8αβ$^+$ IE-T cell subset (Extended Data Fig. 6e), we tested whether CD8αβ$^+$ T cells played a role in restricting the colitogenic GM-CSF response by depleting CD8αβ$^+$ T cells during infection. Staining with a heterologous anti-CD8β antibody clone revealed efficient depletion of CD8αβ$^+$ IE-T cells without any loss of the CD8αα$^+$ IE-T cell subset (Extended Data Fig. 6k). Compared to *Ifngr*$^{\Delta IEC}$ mice given isotype-control antibody, mice depleted of CD8αβ$^+$ T cells showed a significant increase in ATP and GM-CSF (Extended Data Fig. 6l) secretion by the colon explants, which was concomitant with a decrease in colon length at 12 days p.i. (Extended Data Fig. 6m). However, these changes were lower in magnitude than in *Ifngr*$^{\Delta IEC}$ mice, indicating that CD8αβ$^+$ T cells are partially responsible for restraining the ATP–GM-CSF axis and ensuing colitis. Further, the observed decrease in CD39$^+$ IE-T cells in *Ifngr1*$^{\Delta IEC}$ mice was rescued upon transgenic expression of IRF1 in IECs (Extended Data Fig. 6n).

Under homeostasis, colonic IECs express low levels of MHCI, and only a small proportion express MHCII. Although the homeostatic level of epithelial MHCI and MHCII is independent of IFNγR, expression of both MHCI and II is increased in IECs upon *C. rodentium* infection (Extended Data Fig. 1f–i), largely dependent on IFNγR (Fig. 4a and

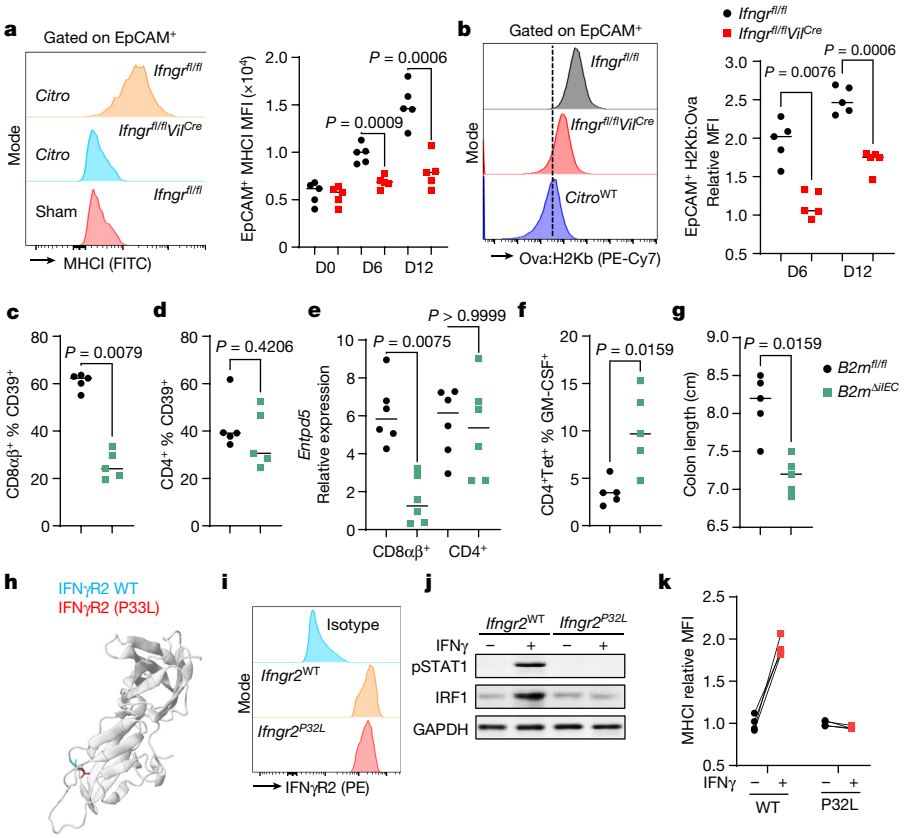

Fig. 4 | IFNγ-mediated antigen presentation by IECs promotes eATPase production by cognate IE-T cells. *Ifngr1*$^{fl/fl}$ and *Ifngr1*$^{fl/fl}$*Vil*^{Cre} mice were infected with *C. rodentium*. **a**, Quantification of MHCI expression on the surface of IECs ($n = 5$ per group). **b**, *Ifngr1*$^{fl/fl}$ and *Ifngr1*$^{fl/fl}$*Vil*^{Cre} mice were infected with *Citro*^{Ova}, and IECs were analysed for the presentation of H2Kb:Ova complex on the surface by flow cytometry ($n = 5$ per group). **c**–**g**, *B2m*$^{fl/fl}$ and *B2m*$^{fl/fl}$*Vil*^{CreERT2} mice were infected with ova-expressing *Citrobacter* on day 0, treated with tamoxifen on days 3–6, and sacrificed on day 12 p.i. Expression of CD39 by CD8αβ$^+$ (**c**) and CD4$^+$ (**d**) IE-T cells ($n = 5$ per group). *Entpd5* expression in purified CD8αβ$^+$ and CD4$^+$ IE-T cells (**e**) ($n = 6$ per group), GM-CSF production from ova-specific CD4$^+$ IE-T cells (**f**) and colon length (**g**) ($n = 5$ per group). Each symbol represents an individual mouse, and the bar represents the median. **h**, Structural prediction by motif analyses. **i**–**k**, Flow cytometric staining for IFNγR2 in WT and *Ifngr2*^{P32L} cell lines (four biological replicates) (**i**). These cells were stimulated with IFNγ and evaluated for STAT1 pTyr701 and IRF1 induction (representative of two independent experiments) (**j**) and MHCI expression on the cell surface by flow cytometry (**k**). Each symbol represents an individual human patient, and the bar represents the median. Data were analysed by ANOVA tests (**a**,**b**) followed by the Dunnet's post hoc test, Mann–Whitney U test (two-sided) (**c**–**g**) or Kruskal–Wallis test followed by Dunn's post-test (**h**,**l**). Scale bar, 100 μm. MFI, median fluorescence intensity.

Extended Data Fig. 7a) and partially rescued by transgenic expression of IRF1 in IFNγR-deficient IECs (Extended Data Fig. 7b,c). To determine whether IECs can present bacterial antigens during colitis, we infected mice with *Citro*^{Ova} and evaluated the presentation of the SIINFEKL-H2Kb (Ova peptide–MHCI) complex on the surface of IECs. Presentation of bacterial peptide–MHCI complexes increased progressively in *Ifngr*$^{fl/fl}$ (WT) IECs and was largely dependent on IFNγR (Fig. 4b) and IRF1 expression in IECs (Extended Data Fig. 7d). Epithelial IFNγR was also required for the presentation of IEC-derived peptides during infection (Extended Data Fig. 7e). These data demonstrate that IECs present bacterial and self-antigens during colitis. CD4$^+$ T cells were the main source of IFNγ (Extended Data Fig. 2o), and their depletion leads to a lower level of epithelial MHCII (Extended Data Fig. 7f), demonstrating that feedback of adaptive immunity onto IECs enhances their antigen presentation capacity.

To directly test whether antigen presentation by IECs contributes to protection against colitis by promoting eATPase expression in IE-T cells, we generated inducible IEC-specific MHCI or MHCII-deficient mice by crossing *Vil*^{creERT2} mice to *b2m*$^{fl/fl}$ mice (that we generated by inserting loxp sites flanking exon 2 of the *b2m* gene using CRISPR–Cas9 mediated gene editing) and *H2ab*$^{fl/fl}$ mice[38], respectively (Extended Data Figs. 8a,b and 9a). Deletion of MHCI or MHCII during days 3–6 p.i. selectively decreased CD39 and *Entpd5* upregulation in CD8αβ$^+$ and CD4$^+$ IE-T cells, respectively (Fig. 4c–e and Extended Data Figs. 8c–e and 9b–g). In line with the abrogation of eATPase production from either CD8αβ$^+$ or CD4$^+$ IE-T cells, deletion of MHCI or MHCII in IECs had an intermediate effect on the ATP–IL-1β–GM-CSF axis (Fig. 4f and Extended Data Figs. 8f–j and 9h–m) and the severity of colitis (Fig. 4g and Extended Data Figs. 8k and 9n,o) when compared to *Ifngr*$^{\Delta IEC}$ mice, which had reduced eATPase expression in both CD8αβ$^+$ and CD4$^+$ IE-T cell subsets (Fig. 3j). In the absence of epithelial MHCI, the production of IFNγ, but not colitogenic GM-CSF, was increased in natural killer cells (Extended Data Fig. 8l). Furthermore, the depletion of natural killer cells did not modulate the colon shortening observed in *B2m*$^{\Delta IIEC}$ mice (Extended Data Fig. 8m,n). Although it is plausible that cell-autonomous antipathogen defence provided by IFNγ signalling[1,39] also promotes protection from colitis, collectively, these data show that IFNγ-dependent antigen presentation by IECs is critical in promoting eATPase expression in IE-T cells on *C. rodentium* infection, which in turn mitigates colitis.

Epithelial IFNγ signalling restrains colitis

To evaluate whether our findings in *C. rodentium*-induced colitis also apply to a non-infectious model of colitis, we subjected the *Ifngr*$^{\Delta IEC}$ and

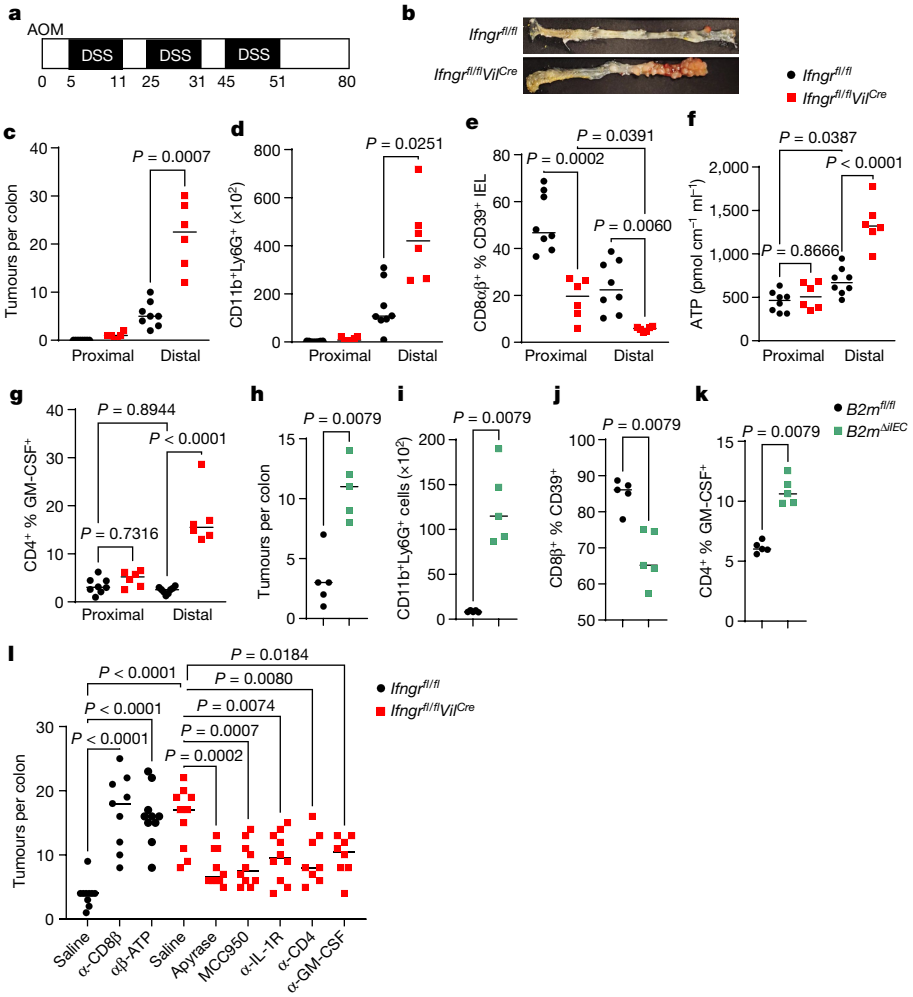

Fig. 5 | IFNγ-mediated antigen presentation restricts colon cancer. *Ifngr1*$^{fl/fl}$ ($n = 8$) *Ifngr1*$^{fl/fl}$*Vil*^{Cre} ($n = 6$) mice were injected with AOM on day 0, followed by administration of 1.5% DSS in drinking water on days 6–11, 25–31 and 45–51; they were sacrificed on day 80. **a**, AOM–DSS treatment model. **b**, Representative pictures of the colon. **c**, Enumeration of tumours in the proximal and distal half of the colon from *Ifngr1*$^{fl/fl}$ ($n = 8$) and *Ifngr1*$^{fl/fl}$*Vil*^{Cre} ($n = 6$) mice at day 80. **d**, Flow cytometric enumeration of infiltrating CD11b$^+$Ly6G$^+$ PMNs. **e**, CD39 expression by CD8αβ$^+$ IE-T cells from proximal and distal half of the colon at day 80. **f**,**g**, Secretion of ATP (**f**) and production of GM-CSF (**g**) from CD4$^+$ IE-T cells from proximal and distal half of the colon from *Ifngr1*$^{fl/fl}$ ($n = 8$) and *Ifngr1*$^{fl/fl}$*Vil*^{Cre} ($n = 6$) mice at day 80. **h**–**k**, *B2m*$^{fl/fl}$ and *B2m*$^{fl/fl}$*Vil*^{CreERT2} mice were administered tamoxifen for five consecutive days and seven days later subjected to AOM–DSS treatment. Enumeration of tumours in the colon (**h**) and flow cytometric analyses of PMN infiltration (**i**), CD39 expression by CD8αβ$^+$ IE-T cells (**j**) and the proportion of GM-CSF-positive CD4$^+$ IE-T cells (**k**) in the distal colon at day 80 ($n = 5$ per group). **l**, Enumeration of tumours in the colons of *Ifngr1*$^{fl/fl}$ and *Ifngr1*$^{fl/fl}$*Vil*^{Cre} mice that were treated with AOM–DSS; administered isotype ($n = 10$), anti-CD8β ($n = 9$), αβ-ATP ($n = 10$), apyrase ($n = 10$), MCC950 ($n = 10$), anti-IL-1R ($n = 10$), anti-CD4 ($n = 8$) or anti-GM-CSF ($n = 8$) on days 9, 11, 13, 26, 28, 30, 32 and 46, 48, 50 and 52 post-AOM; and sacrificed on day 80. Each symbol represents an individual mouse, and the bar represents the median. Data were analysed by ANOVA tests (**c**–**g**,**l**) followed by the Dunnet's post hoc test or Kolmogorov–Smirnov test (**h**–**k**). α, anti.

littermate control mice to a low dose (1%) of dextran sulfate sodium (DSS) for nine days, followed by regular drinking water for three days. Similar to the findings with *C. rodentium* infection, absence of IFNγ sensing by IECs prevented the upregulation of MHCI and MHCII in IECs (Extended Data Fig. 10a,b) and acquisition of CD39 in IE-T cells (Extended Data Fig. 10c,d). As with *C. rodentium* infection, DSS administration in *Ifngr*$^{\Delta IEC}$ mice led to higher activation of the ATP–NLRP3–IL-1β–GM-CSF$^+$CD4$^+$ T cell axis (Extended Data Fig. 10e,f), increased neutrophil infiltration (Extended Data Fig. 10g) and colitis (Extended Data Fig. 10h,i). As with *C. rodentium* infection, antigen presentation by IECs by means of MHCI was also critical in promoting eATPase expression in CD8αβ$^+$ IE-T cells and restricting GM-CSF production by CD4$^+$ T cells and mitigating colitis (Extended Data Fig. 10j–m). Next, we confirmed a pathogenic role for the ATP–NLRP3–IL-1β–GM-CSF$^+$CD4$^+$ T cell axis in DSS-induced colitis by treating *Ifngr*$^{fl/fl}$ mice with αβ-ATP and *Ifngr*$^{\Delta IEC}$ mice with exogenous eATPase, MCC950, anti-IL-1R, anti-GM-CSF or anti-CD4 antibodies during DSS administration (Extended Data Fig. 10n). Taken together, these data expand our findings on the protective role of IFNγ signalling and antigen presentation by IECs to a non-infectious chemical model of colitis.

Perturbed IFNγ signalling is associated with IBD

The SNP rs150137842 in IFNγR2 is significantly associated with the development of CD (allelic frequency 0.000141, $P = 0.0019$, odds ratio 2.81)[40]. Structural prediction by motif analyses[41,42] indicated that this SNP is inactivating, as it perturbs the extracellular domain of the receptor (Fig. 4h). To test the functional effect of this SNP, we introduced the equivalent mutation in a cell line using CRISPR–Cas9 mediated gene editing and treated the mutant and parental cell lines with IFNγ. Consistent with the prediction by structural analysis, the SNP resulted in reduced STAT1 (pTyr701) activation, IRF1 and MHCI upregulation

after stimulation with IFNγ without affecting the expression of IFNγR2 itself (Fig. 4i–k). These findings are in line with observations showing that decreased abundance of CD39$^+$ IE-T cells is associated with paediatric IBD[43] and that SNPs in the promoter of ENTPD1 (CD39) leading to lower CD39 expression are associated with IBD[44]. Although it remains to be tested whether IBD patients with these mutations are resistant to current IBD therapies, the *Ifngr*$^{\Delta IEC}$ mice were resistant to tumour necrosis factor (TNF) blockade (Fig. 2g), demonstrating this to be a model of anti-TNF refractory colitis. Taken together, these data indicate that a defect in IFNγ signalling may promote IBD by failing to regulate extracellular ATP and thereby promoting colitogenic T cell responses.

Epithelial IFNγ signalling is protective in colon cancer

IBD increases the risk of developing colorectal cancer[45]. To evaluate whether the epithelial antigen presentation pathway is relevant in colorectal cancer, we subjected IEC-specific IFNγR-deficient mice to DNA-damaging agent azoxymethane (AOM) followed by cyclic oral administration of DSS (Fig. 5a). Mice with IEC-specific deletion of *Ifngr1* had significantly increased tumour counts compared to the littermate controls (Fig. 5b,c). As most of the tumours in both *Ifngr*$^{fl/fl}$ and *Ifngr*$^{\Delta IEC}$ mice were restricted to the distal half of the colon (Fig. 5c), which is a feature of the AOM–DSS model[46,47], we analysed the immune responses following AOM–DSS treatment in the proximal and distal colon separately. The distal colons of the *Ifngr*$^{\Delta IEC}$ mice had increased numbers of neutrophils (Fig. 5d) and decreased production of CD39 from CD8αβ$^+$ IE-T cells (Fig. 5e), which correlated with increased secretion of ATP from distal colon explants (Fig. 5f) and increased production of GM-CSF from CD4$^+$ IE-T cells (Fig. 5g). To test the individual contribution of epithelial MHCI to the pathogenesis of colorectal cancer, we treated IEC-specific β2m-deficient mice with AOM–DSS. *B2m*$^{i\Delta IEC}$ mice had an increased number of tumours and neutrophils in the distal colon compared to the respective littermate control mice (Fig. 5h–j), but to a moderate extent compared to *Ifngr*$^{\Delta IEC}$ mice (Fig. 5c–g). Furthermore, deletion of epithelial MHCI led to lower upregulation of CD39 in CD8αβ$^+$ IE-T cells (Fig. 5j) and increased GM-CSF production from CD4$^+$ IE-T cells (Fig. 5k).

To directly test whether these alterations are relevant to disease pathogenesis, we treated *Ifngr*$^{fl/fl}$ mice with anti-CD8β or αβ-ATP and *Ifngr*$^{\Delta IEC}$ mice with exogenous ATPase, MCC950, anti-IL-1R or anti-CD4 during DSS administration stages of the AOM–DSS protocol. Although anti-CD8β or αβ-ATP treatment in *Ifngr*$^{fl/fl}$ mice increased the tumour burden, depletion of extracellular ATP, GM-CSF or CD4$^+$ T cells or blockade of IL-1R or inhibition of NLRP3 mitigated the tumour burden in the colons of *Ifngr*$^{\Delta IEC}$ mice (Fig. 5l). Therefore, IFNγ-mediated antigen presentation protects from colorectal cancer by promoting eATPase production from T cells and restraining overt NLRP3 activation, IL-1 and GM-CSF production.

Discussion

Our work puts forward a mechanism through which IECs induce IE-T cells with anti-inflammatory protective functions. More specifically, our findings reveal that IFNγ sensing and MHCI antigen presentation by epithelial cells promote eATPase expression in CD8αβ$^+$ IE-T cells that in turn control the extracellular level of ATP, NLRP3 inflammasome activation and development of a pathogenic GM-CSF$^+$CD4$^+$ T cell response (Extended Data Fig. 11). These findings about the role of IFNγ signalling and antigen presentation, along with IFNγ-mediated cell-autonomous defence mechanisms[1,39] by tissue cells, may be more generally relevant to autoimmune and inflammatory diseases in which GM-CSF$^+$CD4$^+$ T cell responses are thought to play a pathogenic role. Biologics and inhibitors targeting IL-1β (ref. 48), NLRP3 (ref. 49) or GM-CSF[50] are now used in the clinic or clinical trials against non-IBD inflammatory diseases. Our studies indicate that they may be also effective in treating IBD and CRC, especially when patients express SNPs in the IFNγ signalling pathway or are resistant to other current therapies.

Online content

Any methods, additional references, Nature Portfolio reporting summaries, source data, extended data, supplementary information, acknowledgements, peer review information; details of author contributions and competing interests; and statements of data and code availability are available at https://doi.org/10.1038/s41586-023-06721-1.

1. Ivashkiv, L. B. IFNγ: signalling, epigenetics and roles in immunity, metabolism, disease and cancer immunotherapy. *Nat. Rev. Immunol.* **18**, 545–558 (2018).
2. Dahlhamer, J. M. Prevalence of inflammatory bowel disease among adults aged≥ 18 years—United States, 2015. *MMWR Morb. Mortal. Wkly. Rep.* **65**, 1166–1169 (2016).
3. Kappelman, M. D., Moore, K. R., Allen, J. K. & Cook, S. F. Recent trends in the prevalence of Crohn's disease and ulcerative colitis in a commercially insured US population. *Dig. Dis. Sci.* **58**, 519–525 (2013).
4. Kim, E. R. & Chang, D. K. Colorectal cancer in inflammatory bowel disease: the risk, pathogenesis, prevention and diagnosis. *World J. Gastroenterol.* **20**, 9872–9881 (2014).
5. Podolsky, D. K. & Isselbacher, K. J. Glycoprotein composition of colonic mucosa. Specific alterations in ulcerative colitis. *Gastroenterology* **87**, 991–998 (1984).
6. Rhodes, J. M. Unifying hypothesis for inflammatory bowel disease and associated colon cancer: sticking the pieces together with sugar. *Lancet* **347**, 40–44 (1996).
7. Rabinowitz, K. & Mayer, L. Working out mechanisms of controlled/physiologic inflammation in the GI tract. *Immunol. Res.* **54**, 14–24 (2012).
8. Platanias, L. C. Mechanisms of type-I-and type-II-interferon-mediated signalling. *Nat. Rev. Immunol.* **5**, 375–386 (2005).
9. Alspach, E., Lussier, D. M. & Schreiber, R. D. Interferon γ and its important roles in promoting and inhibiting spontaneous and therapeutic cancer immunity. *Cold Spring Harb. Perspect. Biol.* **11**, a028480 (2019).
10. Castro, F., Cardoso, A. P., Gonçalves, R. M., Serre, K. & Oliveira, M. J. Interferon-gamma at the crossroads of tumor immune surveillance or evasion. *Front. Immunol.* **9**, 847 (2018).
11. Zhou, Z. et al. Type III interferon (IFN) induces a type I IFN-like response in a restricted subset of cells through signaling pathways involving both the Jak-STAT pathway and the mitogen-activated protein kinases. *J. Virol.* **81**, 7749–7758 (2007).
12. Jostins, L. et al. Host–microbe interactions have shaped the genetic architecture of inflammatory bowel disease. *Nature* **491**, 119–124 (2012).
13. Lu, S. et al. Single nucleotide polymorphisms within interferon signaling pathway genes are associated with colorectal cancer susceptibility and survival. *PLoS ONE* **9**, e111061 (2014).
14. Koroleva, E. P. et al. Citrobacter rodentium-induced colitis: a robust model to study mucosal immune responses in the gut. *J. Immunol. Methods* **421**, 61–72 (2015).
15. Bouladoux, N., Harrison, O. J. & Belkaid, Y. The mouse model of infection with Citrobacter rodentium. *Curr. Protoc. Immunol.* **119**, 19.15.11–19.15.25 (2017).
16. Raczynski, A. R. et al. Enteric infection with Citrobacter rodentium induces coagulative liver necrosis and hepatic inflammation prior to peak infection and colonic disease. *PLoS ONE* **7**, e33099 (2012).
17. Ivanov, I. I. et al. Induction of intestinal Th17 cells by segmented filamentous bacteria. *Cell* **139**, 485–498 (2009).
18. Basu, R. et al. Th22 cells are an important source of IL-22 for host protection against enteropathogenic bacteria. *Immunity* **37**, 1061–1075 (2012).
19. Guy-Grand, D. et al. Origin, trafficking, and intraepithelial fate of gut-tropic T cells. *J. Exp. Med.* **210**, 1839–1854 (2013).
20. Mortha, A. et al. Microbiota-dependent crosstalk between macrophages and ILC3 promotes intestinal homeostasis. *Science* **343**, 1249288 (2014).
21. Pearson, C. et al. ILC3 GM-CSF production and mobilisation orchestrate acute intestinal inflammation. *eLife* **5**, e10066 (2016).
22. Griseri, T. et al. Granulocyte macrophage colony-stimulating factor-activated eosinophils promote interleukin-23 driven chronic colitis. *Immunity* **43**, 187–199 (2015).
23. Schnell, A. et al. Stem-like intestinal Th17 cells give rise to pathogenic effector T cells during autoimmunity. *Cell* **184**, 6281–6298.e6223 (2021).
24. Hamilton, J. A. GM-CSF in inflammation. *J. Exp. Med.* https://doi.org/10.1084/jem.20190945 (2020).
25. Hu, Y. et al. Interleukin-1β-induced IRAK1 ubiquitination is required for TH-GM-CSF cell differentiation in T cell-mediated inflammation. *J. Autoimmun.* **102**, 50–64 (2019).
26. Ronchi, F. et al. Experimental priming of encephalitogenic Th1/Th17 cells requires pertussis toxin-driven IL-1β production by myeloid cells. *Nat. Commun.* **7**, 1–11 (2016).
27. Sharma, D. & Kanneganti, T.-D. The cell biology of inflammasomes: mechanisms of inflammasome activation and regulation. *J. Cell Biol.* **213**, 617–629 (2016).
28. Rathinam, V. A., Vanaja, S. K. & Fitzgerald, K. A. Regulation of inflammasome signaling. *Nat. Immunol.* **13**, 333–342 (2012).
29. Malik, A. & Kanneganti, T. D. Function and regulation of IL-1α in inflammatory diseases and cancer. *Immunol. Rev.* **281**, 124–137 (2018).
30. Pizzirani, C. et al. Stimulation of P2 receptors causes release of IL-1β–loaded microvesicles from human dendritic cells. *Blood* **109**, 3856–3864 (2007).
31. Baroni, M. et al. Stimulation of P2 (P2X7) receptors in human dendritic cells induces the release of tissue factor-bearing microparticles. *FASEB J.* **21**, 1926–1933 (2007).
32. Mariathasan, S. et al. Cryopyrin activates the inflammasome in response to toxins and ATP. *Nature* **440**, 228–232 (2006).
33. Atarashi, K. et al. ATP drives lamina propria TH 17 cell differentiation. *Nature* **455**, 808–812 (2008).

34. Yona, S. et al. Fate mapping reveals origins and dynamics of monocytes and tissue macrophages under homeostasis. *Immunity* **38**, 79–91 (2013).
35. Robson, S. C., Sévigny, J. & Zimmermann, H. The E-NTPDase family of ectonucleotidases: structure function relationships and pathophysiological significance. *Purinergic Signal.* **2**, 409 (2006).
36. Zadran, S., Amighi, A., Otiniano, E., Wong, K. & Zadran, H. ENTPD5-mediated modulation of ATP results in altered metabolism and decreased survival in gliomablastoma multiforme. *Tumor Biol.* **33**, 2411–2421 (2012).
37. Feldbrügge, L. et al. Expression of ecto-nucleoside triphosphate diphosphohydrolases-2 and-3 in the enteric nervous system affects inflammation in experimental colitis and Crohn's disease. *J. Crohns Colitis* **11**, 1113–1123 (2017).
38. Hashimoto, K., Joshi, S. K. & Koni, P. A. A conditional null allele of the major histocompatibility IA-beta chain gene. *Genesis* **32**, 152–153 (2002).
39. Huang, S., Meng, Q., Maminska, A. & MacMicking, J. D. Cell-autonomous immunity by IFN-induced GBPs in animals and plants. *Curr. Opin. Immunol.* **60**, 71–80 (2019).
40. Lim, E. T. et al. Distribution and medical impact of loss-of-function variants in the Finnish founder population. *PLoS Genet.* **10**, e1004494 (2014).
41. Khanna, T., Hanna, G., Sternberg, M. J. & David, A. Missense3D-DB web catalogue: an atom-based analysis and repository of 4M human protein-coding genetic variants. *Hum. Genet.* **140**, 805–812 (2021).
42. Ittisoponpisan, S. et al. Can predicted protein 3D structures provide reliable insights into whether missense variants are disease associated? *J. Mol. Biol.* **431**, 2197–2212 (2019).
43. Huang, B. et al. Mucosal profiling of pediatric-onset colitis and IBD reveals common pathogenics and therapeutic pathways. *Cell* **179**, 1160–1176 (2019).
44. Friedman, D. J. et al. CD39 deletion exacerbates experimental murine colitis and human polymorphisms increase susceptibility to inflammatory bowel disease. *Proc. Natl Acad. Sci. USA* **106**, 16788–16793 (2009).
45. Howlader, N. et al. *SEER Cancer Statistics Review, 1975–2018* (National Cancer Institute, 2021).
46. Parang, B., Barrett, C. W. & Williams, C. S. in *Gastrointestinal Physiology and Diseases* (ed. Ivanov, A. I.) 297–307 (Springer, 2016).
47. Malik, A. et al. SYK-CARD9 signaling axis promotes gut fungi-mediated inflammasome activation to restrict colitis and colon cancer. *Immunity* **49**, 515–530 (2018).
48. Ridker, P. M. et al. Antiinflammatory therapy with canakinumab for atherosclerotic disease. *N. Engl. J. Med.* **377**, 1119–1131 (2017).
49. Klück, V. et al. Dapansutrile, an oral selective NLRP3 inflammasome inhibitor, for treatment of gout flares: an open-label, dose-adaptive, proof-of-concept, phase 2a trial. *Lancet Rheumatol.* **2**, e270–e280 (2020).
50. Lotfi, N. et al. Roles of GM-CSF in the pathogenesis of autoimmune diseases: an update. *Front. Immunol.* **10**, 1265 (2019).

Methods

Mice

Mice used in these studies are on the C57BL/6 background and were maintained under specific pathogen-free conditions at the University of Chicago. *Ifngr1*$^{fl/fl}$, *H2ab*$^{fl/fl}$, *Vil*^{Cre} and *Vil*^{CreERT2} mice have been described previously[38,51–53]. *B2m*$^{fl/fl}$, *R26*^{LSLOva} and *R26*^{LSLIrf1} mice were generated on C56BL/6J background by CRISPR–Cas9-mediated genetic editing using guide RNAs and homology-directed repair (HDR) donor sequences indicated in supplementary information. *R26*^{LSLOva} and *R26*^{LSLIrf1} mice were generated by inserting the *ovalbumin* or *Irf1* coding sequence, respectively, into the *Rosa 26* locus downstream of the hybrid CAG promoter and a stop cassette flanked by the Cre-target loxP sites (CAG-loxp-stop-loxp-Ova) in C57BL/6J zygotes. The AOM–DSS murine model for colorectal tumorigenesis has been previously described[54]. For the DSS model of colitis, mice were administered the indicated dose of DSS (mol wt 36–40 kDa; Alfa Aesar) for nine days, followed by regular water. For antibody injections, mice were injected with 50 μg of anti-CD4 or GM-CSF or 200 μg or anti-IL-1R from Bio-X-Cell in 200 μl sterile saline every other day by means of intraperitoneal injections. Apyrase (200 U, A2230) and αβ-ATP (500 μg, M6517) and MCC950 (40 mg per kg CP-456773) from Sigma were injected daily for colitis experiments and every other day for CRC experiments by intraperitoneal injections in 200 μl saline. *C. rodentium* strain DBS100 was grown at 37 °C in Luria broth under agitation. Overnight cultures were diluted to 10^{10} colony-forming units per ml in sterile saline, and 200 μl of it was administered to mice seven to eight weeks of age by intragastric gavage. Data are representative of one or two independent experiments with two-sided *P* values. Mice were allocated to experimental groups on the basis of their genotype and randomized in the given age-matched group. Given that our mice were inbred and matched for age, we always assumed similar variance between the different experimental group. We did not perform an a priori sample-size estimation but always used as many mice per group as possible in an attempt to minimize type I and type II errors. Mice were used at seven or eight weeks of age, with similar numbers of males and females. The University of Chicago Animal Resource Committee approved all animal study protocols.

Generation of ova-expressing *Citrobacter*

To make an ova-expressing *Citrobacter rodentium* strain, we cloned an artificial and constitutive Enterobacteriaceae-specific promoter upstream of ovalbumin coding sequence and terminator sequence into the temperature-sensitive transposase 7 attachment site (*attTn7*) targeting vector. Then this vector was electroporated into *C. rodentium DSB100*. Growth at permissive temperature along with constitutive expression of the recombination machinery led to the integration of the promoter-ova-terminator sequence into the *attTn7* site. Next, the plasmid was cured by subsequent growth at non-permissive temperatures. Site-specific integration was confirmed by sequencing from the neighbouring *glmS* region of the *attTntn7* locus, and the expression of ova was confirmed by western blotting and intracellular staining (Extended Data Fig. 3a–d). Constitutive expression from the genome, unlike expression from a plasmid, obviates the need to administer antibiotics to mice to maintain the selection of the plasmid. It therefore allows tracking of the pathogen-specific T cell responses by ova-specific tetramers without needing to induce antibiotic-mediated dysbiosis in the mice.

Histology and microscopy analysis

Colons were fixed in 10% formalin, embedded in paraffin, sectioned with 5 μm thickness, and stained with haematoxylin and eosin (H&E). Histological scoring was conducted as described previously[55]. 4: presence of erosions, 3: intense inflammation with clusters of neutrophils, 2: neutrophils in lamina propria or in epithelium with goblet cell loss, 1: moderate lamina propria lymphoplasmacytic inflammation or mucosal thickening, 0: normal. The sections were imaged using the CRi Panoramic MIDI ×20 whole-slide scanner.

Measurement of cytokine levels

Cytokines in colon explants and homogenates were measured by enzyme-linked immunosorbent assay (ELISA). The culture of colon explants was described previously[56]. Briefly, for explant culture, 0.5 cm of the distal colon was incubated in IMDM media supplemented with 10% fetal bovine serum (FBS) and penicillin, streptomycin and gentamycin for 24 h. Explants were also weighed before incubation, and equivalent data were obtained if the cytokine levels were normalized to their wet weight. The IL-1β and GM-CSF ELISA kits were obtained from eBioscience and used according to manufacturers' instructions. The levels of ATP from colon explants after 30 min of incubation were determined with an ATP assay kit (Abcam) according to the manufacturer's instructions, except that the cell lysis step was omitted.

Flow cytometry analysis

Single-cell suspensions were prepared from the colon as previously described[56]. Briefly, to remove epithelial cells, the colon was washed and cut into small pieces, and the pieces were incubated with calcium- and magnesium-free Hank's balanced salt solution supplemented with 5% FBS and 5 mM ethylenediaminetetraacetic acid (EDTA, Sigma-Aldrich) and centrifuged at 140 rpm at 25 °C for 30 min. Tissues were then incubated with RPMI 1640 containing 10% FBS and 0.5 mg ml^{-1} collagenase type IV for 1 h at 37 °C with shaking at 150 pm. Liberated cells were collected by passage through a 70 μm nylon mesh. Isolated cells from the EDTA-treated (epithelial) and collagenase-treated (lamina propria) fractions were separated on a 40%/80% discontinuous Percol gradient (GE Bioscience).

Colon, spleen and MLN cells were processed and stimulated as previously described[56]. Briefly, single-cell suspensions were prepared and stimulated with phorbol-12-myristate-13-acetate and ionomycin for 4 h, with brefeldin A (00-4506, Affymetrix eBioscience) added for the last 2 h. For intracellular cytokine staining, cells were fixed and permeabilized by using a fixation and permeabilization kit (00-5523, eBioscience).

Antibodies used were CD45 Pac Blue (30-F11) Biolegend catalogue no. 103126, TCRgd FITC (eBioGL3) Thermo Fisher catalogue no. 11-5711-82, CD4 BV785 (GK1.5) Biolegend catalogue no. 100453, CD4 BV605 (GK1.5) Biolegend catalogue no. 100451, CD8β BUV395 (H35-17.2) BD catalogue no. 740278, CD8α PerCp/Cy5.5 (53-6.7) BD catalogue no. 551162, NK1.1 PE-CF594 (PK136) BD catalogue no. 562864, TCRβ BUV737 (H57-597) BD catalogue no. 612821, TCRβ BV711 (H57-597) BD catalogue no. 563135, CD3ε BUV737 (145-2C11) BD catalogue no. 612771, IFNγ APC (XMG1.2) BD catalogue no. 554413, IL-10 PEcy7 (JES5-16E3) Biolegend catalogue no. 505026, IL-17a PE (ebio17B7) Thermo Fisher catalogue no. 12-7177-81, CD45.2 BUV395 (104) BD catalogue no. 553772, RORγt BV786 (Q31-37) BD catalogue no. 564723, FOXP3 eflour450 (FJK-16s) Thermo Fisher catalogue no. 48-5773-82, FOXP3 FITC (FJK-16s) Thermo Fisher catalogue no. 11-5773-82, Tbet PE (4B10) Biolegend catalogue no. 644810, CD44 PE-CY7 (IM7) Biolegend catalogue no. 103030, CD62L PE (MEL-14) Biolegend catalogue no. 104408, Epcam PerCp/Cy5.5 (G8.8) Biolegend catalogue no. 18220, CD19 FITC (1D3/CD19) Biolegend catalogue no. 152404, NK1.1 BV605 (PK136) Biolegend catalogue no. 108753, CD11C BV605 (N418) Biolegend catalogue no. 117334, TER119 BV605 (TER-119) Biolegend catalogue no. 116239, F4/80 BV605 (BM8) Biolegend catalogue no. 123133, CD3ε BV605 (145-2C11) Biolegend catalogue no. 100351, Ly6G BV605 (1A8) Biolegend catalogue no. 127639, CD39 SB436 (24DMS1) Invitrogen catalogue no. 62-0391-82, GM-CSF PE-CF594 (MP1-22E9) BioLegend catalogue no. 505422. Antibodies were used at 1:200 dilution. Ova-specific tetramers (10 μg ml^{-1}) were obtained by the NIH tetramer core facility and added during cell stimulation. Flow cytometry data were acquired on an Aurora cytometer with SpectroFlo software (Cytek Biosciences) and analysed with FlowJo v.10 software (TreeStar).

Western blotting

Proteins were extracted from colon tissues using radioimmunoprecipitation assay lysis buffer supplemented with proteinase and phosphatase inhibitors (Roche). Samples were resolved by 8%–15% sodium dodecyl sulfate-polyacrylamide gel electrophoresis and transferred onto polyvinylidene difluoride membranes. Blocking was performed in 3% bovine serum albumin in trisbuffered saline with Tween-20 for 1 h, and membranes were incubated with primary antibodies Phospho-Stat1 (Tyr701) (58D6) no. 9167, IRF1 (D5E4) XP no. 8478 or GAPDH (D16H11) XP no. 5174 from Cell Signalling technology at 1:1,000 dilution overnight at 4 °C. Membranes were incubated with IRD680–conjugated secondary antibody (925-68071, LI-COR) for 1 h (1:10,000 dilution), and proteins were visualized by using the LI-COR Odyssey imager.

Cell culture, generation of *Ifngr2*^{P32L} cell line and stimulations

B16 cells were cultured in Dulbecco's Modified Eagle Medium with 10% FBS as described previously[57]. Cells were stimulated with 10 ng ml^{-1} of recombinant IFNγ (R&D systems) for 30 mins for immunoblotting and 4 h for fluorescence-activated cell sorting. For the generation of the IFNγR P32L SNP, cells at 40%–50% confluency were transfected with the ribonucleoprotein (RNP) mixture containing 1 μM of the guide RNA, HDR template and Cas9 (IDT) with FugeneHD transfection reagent (Promega) as per the manufacturer's instructions.

Quantitative real-time PCR

RNA was isolated by using the RNeasy kit (Sigma-Aldrich) as per the manufacturer's instructions and converted into cDNA as previously described[58]. Gene expression was assessed by using the 2× SYBR Green master mix as per the manufacturer's instructions (Applied Biosystems). Sequences for quantitative reverse transcription-polymerase chain reaction (qRT-PCR) primers are listed in the resource table. qRT-PCR data were analysed by the $2^{-\Delta\Delta CT}$ method, with β-actin as the housekeeping gene. Oligonucleotides were as follows:

GAPDH forward: AGGTCGGTGTGAACGGATTTG
GAPDH reverse: TGTAGACCATGTAGTTGAGGTCA
IFNγ forward: ATGAACGCTACACACTGCATC
IFNγ reverse: TCTAGGCTTTCAATGACTGTGC
IRF1 forward: ATGCCAATCACTCGAATGCG
IRF1 reverse: TTGTATCGGCCTGTGTGAATG
Entpd1 forward: AAGGTGAAGAGATTTTGCTCCAA
Entpd1 reverse: TTTGTTCTGGGTCAGTCCCAC
Entpd5 forward: TTGGCAGCACTGTCTTCTACA
Entpd5 reverse: GCCCGCATCAAACATAATTCC

Statistical analysis

Statistical significance for datasets was determined by parametric or non-parametric tests when appropriate and is indicated in the respective figure legends. $P < 0.05$ was considered significant.

Reporting summary

Further information on research design is available in the Nature Portfolio Reporting Summary linked to this article.

Data availability

Source data are provided with this paper.

51. Lee, S. H. et al. Identifying the initiating events of anti-Listeria responses using mice with conditional loss of IFN-γ receptor subunit 1 (IFNGR1). *J. Immunol.* **191**, 4223–4234 (2013).
52. Madison, B. B. et al. Cis elements of the villin gene control expression in restricted domains of the vertical (crypt) and horizontal (duodenum, cecum) axes of the intestine. *J. Biol. Chem.* **277**, 33275–33283 (2002).
53. el Marjou, F. et al. Tissue-specific and inducible Cre-mediated recombination in the gut epithelium. *Genesis* **39**, 186–193 (2004).
54. Malik, A. et al. IL-33 regulates the IgA-microbiota axis to restrain IL-1α–dependent colitis and tumorigenesis. *J. Clin. Invest.* **126**, 4469–4481 (2016).
55. Marchal-Bressenot, A. et al. Development and validation of the Nancy histological index for UC. *Gut* **66**, 43–49 (2017).
56. Malik, A., Sharma, D., St Charles, J., Dybas, L. & Mansfield, L. Contrasting immune responses mediate Campylobacter jejuni-induced colitis and autoimmunity. *Mucosal Immunol.* **7**, 802–817 (2014).
57. Lupfer, C. et al. Receptor interacting protein kinase 2-mediated mitophagy regulates inflammasome activation during virus infection. *Nat. Immunol.* **14**, 480–488 (2013).
58. Sharma, D., Malik, A., Steury, M. D., Lucas, P. C. & Parameswaran, N. Protective role of β-arrestin2 in colitis through modulation of T-cell activation. *Inflam. Bowel Dis.* **21**, 2766–2777 (2015).
59. McKenzie, G. J. & Craig, N. L. Fast, easy and efficient: site-specific insertion of transgenes into Enterobacterial chromosomes using Tn 7 without need for selection of the insertion event. *BMC Microbiol.* **6**, 39 (2006).

Acknowledgements This work was supported by the US National Institutes of Health (R01DK067180) to B.J., the University of Chicago's Center for Interdisciplinary Study of Inflammatory Intestinal Disorders (C-IID) Pilot & Feasibility Award (NIDDK P30 DK042086) to A.M. and D.S., Crohn's and Colitis Foundation Career Development Award no. 964209 to A.M. and a G.I. Research Foundation Associates Board Award to A.M. and D.S. Whole-slide scanning was performed by S. Bond and K. Rodriguez in the Integrated Light Microscopy Core at the University of Chicago, which receives financial support from a Cancer Center Support Grant (P30CA014599), RRID:SCR_019197. We thank the University of Chicago Transgenic Mouse Facility (RRID:SCR_019171), especially L. Degenstein, for their assistance with producing the mice used in this study. We thank W. Lisicka, N. Usher, C. Ciszewski, Human Disease and Immune Discovery core (RRID:SCR_022936) and members of the B. Jabri lab at the University of Chicago. The model figure (Extended Data Fig. 11) was created with BioRender.com.

Author contributions A.M. and B.J. conceptualized this work. A.M., D.S., R.A.-G., C.W., S.Z. and S.M. developed the methodology. A.M., D.S., S.Z. and S.M. performed the investigation. A.M., D.S., S.M. and B.J. did the formal analysis. A.M. wrote the original draft, and D.S. and B.J. reviewed and edited it. A.M. and B.J. acquired the funding and resources. B.J. supervised the study.

Competing interests The authors declare no competing interests.

Additional information

Supplementary information The online version contains supplementary material available at https://doi.org/10.1038/s41586-023-06721-1.

Correspondence and requests for materials should be addressed to Ankit Malik or Bana Jabri.

Peer review information *Nature* thanks Oliver Pabst and the other, anonymous, reviewer(s) for their contribution to the peer review of this work.

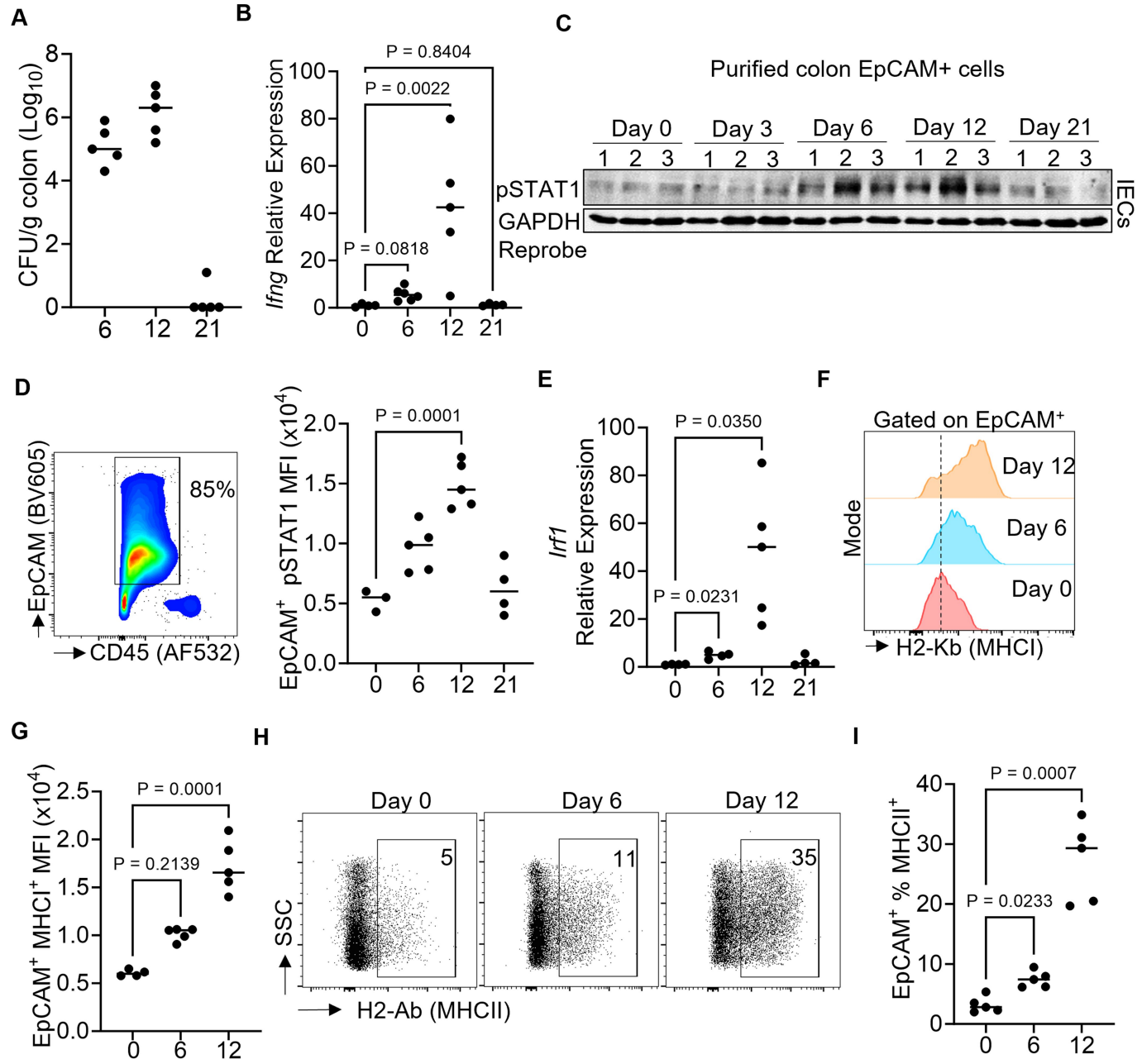

Extended Data Fig. 1 | Progressive increase in IFN-γ signaling and antigen presentation by IECs during colitis. C57BL/6 J mice were infected with *Citrobacter rodentium*. **(A)** *Citrobacter* colonization in the colon (n = 5 per group) and **(B)** quantification of *Ifng* transcript in colon tissue by RT-PCR (n = 4 for d0 and d21, n = 6 for d6 and n = 5 for d12). STAT1 pTyr701 analyses in IECs by **(C)** immunoblotting, representative of two independent experiments and **(D)** flow cytometry (n = 3 for d0, n = 6 for d6 and n = 5 for d12 and n = 4 for d21). **(E)** Quantification of *Irf1* transcript in purified IECs (EpCAM$^+$) by RT-PCR (n = 4 for d0, d6 and d21, n = 5 for d12). Flow cytometric analyses for (**F** and **G**) MHCI (n = 4 for d0, n = 5 for d6 and d12) and (**H** and **I**) MHCII (n = 4 for d0, n = 5 for d6 and d12) in the IECs from colons of mice at indicated day post-infection. **(J)** Colon histology score in *Ifngr1*$^{fl/fl}$ and *Ifngr1*$^{fl/fl}$ *Vil*^{Cre} mice. The horizontal bar represents the median, and each symbol and each lane in the immunoblot represents an individual mouse. Data were analyzed by **(A, B, D, E, G** and **I)** Brown-Forsthye and Welsch ANOVA tests followed by the Dunnet's post-hoc test.

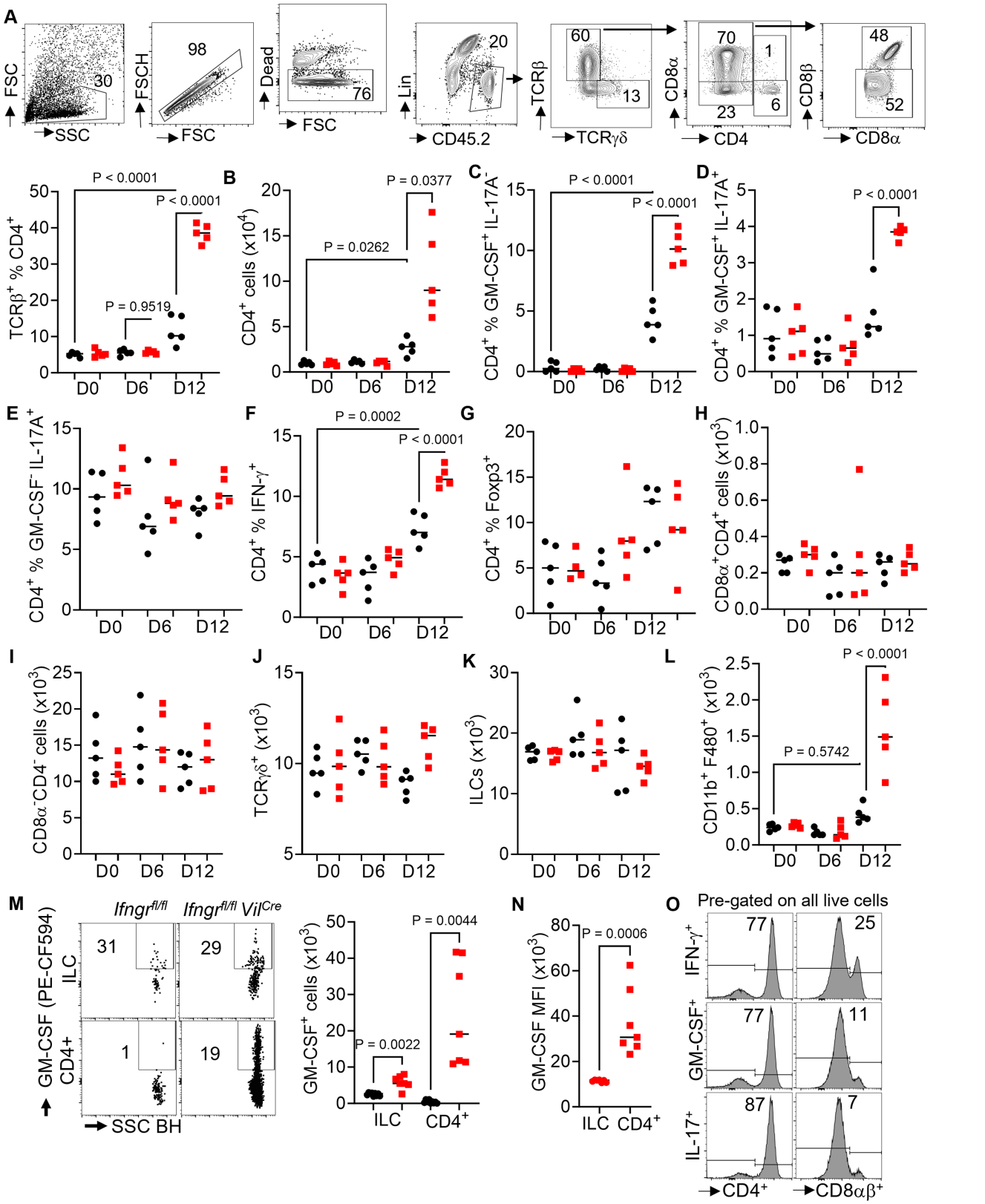

Extended Data Fig. 2 | Epithelial sensing of IFN-γ orchestrates T cell responses during colitis. (A-I) *Ifngr1*$^{fl/fl}$ and *Ifngr1*$^{fl/fl}$ *Vil*^{Cre} mice were infected with *Citrobacter rodentium* (n = 5 per group). **(A-B)** Enumeration of I.E. CD4$^+$ T cells and **(C-G)** evaluation of production of indicated factors by them at indicated days post-infection. Enumeration of **(H-L)** indicated cells in the epithelium. **(M)** Comparison of GM-CSF production from ILCs and CD4$^+$ T cells (n = 7 per group) and **(N)** GM-CSF MFI in ILCs and CD4$^+$ T cells in epithelium of *Ifngr1*$^{fl/fl}$ *Vil*^{Cre} mice at day 12 p.i. (n = 7 per group). **(O)** The indicated factors were gated globally on the live cell gate and then analyzed for the contribution of CD8αβ$^+$ or CD4$^+$ colonic IE-T cells in their production. Each symbol represents an individual mouse, and the bar indicates the median. Data were analyzed by **(A-L)** ANOVA followed by the Holm–Sidak post-hoc test or (**M-N**) Mann-Whitney U test (two-sided). MFI, median fluorescence intensity.

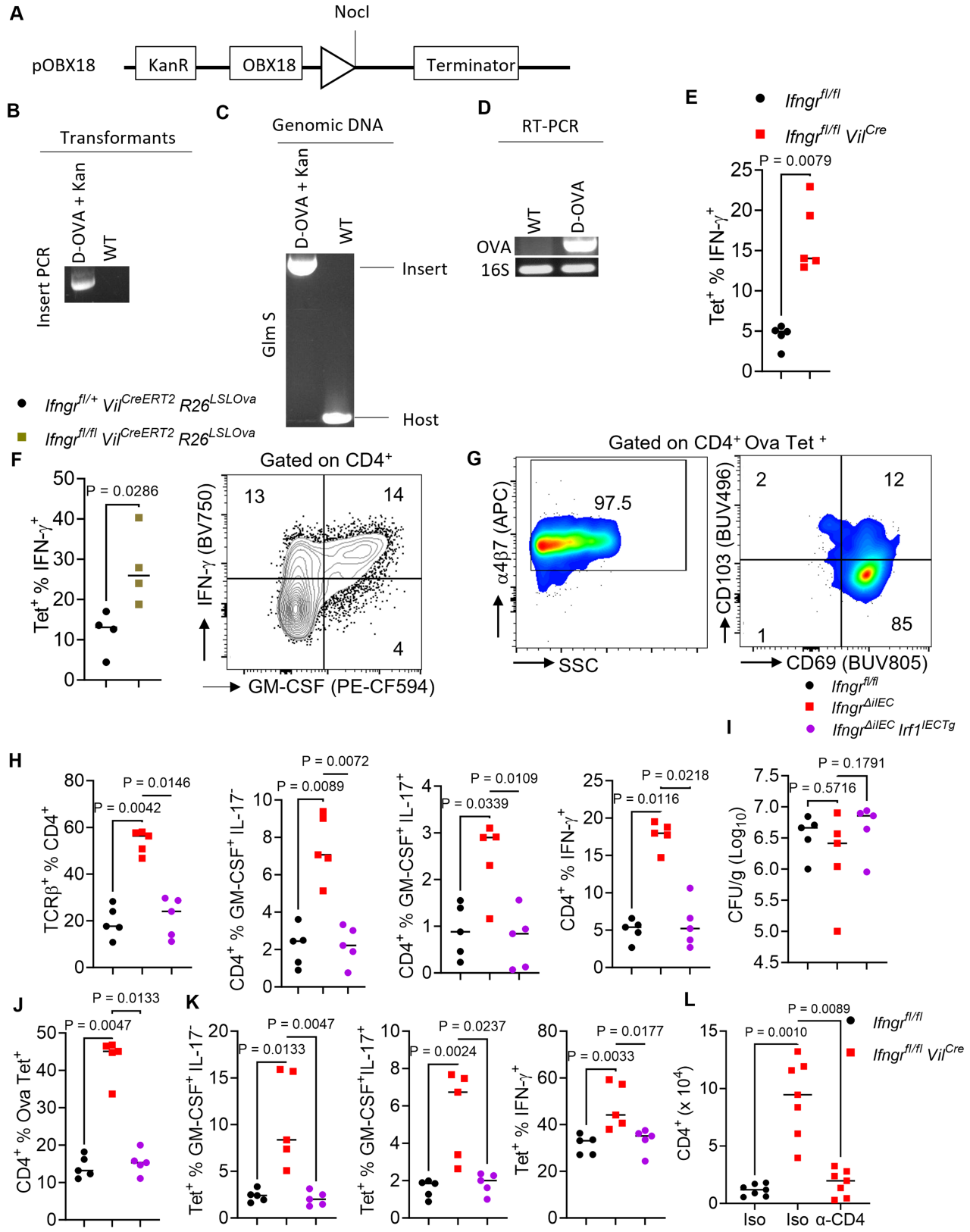

Extended Data Fig. 3 | See next page for caption.

Extended Data Fig. 3 | Generation of the ovalbumin-expressing strain of *C. rodentium* and characterization of ova-specific IE-T cells. Ovalbumin coding sequence was cloned into the NocI site of pOBX18 plasmid containing the artificial and constitutive Enterobacteriaceae-specific promoter and terminator sequence into the temperature-sensitive transposase 7 attachment site (*attTn7*) targeting vector (vector described in[59]) (**A**) plasmid map and (**B**) gel picture of the transformed vector. Then, this vector was electroporated into *C. rodentium*. Growth at permissive temperature along with constitutive expression of the recombination machinery led to the integration of the promoter-ova-terminator sequence into the *attTn7* site. Next, the plasmid was cured by subsequent growth at non-permissive temperatures. Site-specific integration was confirmed by (**C**) PCR and sequencing from the neighboring *glmS* region of the *attTntn7* locus and the expression of ova was confirmed by (**D**) RT-PCR, representative of two independent clones. **(E)** *Ifngr1*$^{fl/fl}$ and *Ifngr1*$^{fl/fl}$ *Vil*^{Cre} mice were infected with ova^{+} *Citrobacter* and (**F**) *Ifngr*$^{fl/fl}$ *Vil*^{creERT2} *Ova*^{Tg} and *Ifngr*$^{fl/+}$ *Vil*^{creERT2} *Ova*^{Tg} mice were infected with wild-type *Citrobacter* and administered tamoxifen on days 3-6 p.i and evaluated for IFN-γ production from the ova-specific CD4^{+} IE-T cells (n = 4 per group). **(G)** Flow cytometric phenotyping of ova-specific CD4^{+} IE-T cells at day 12 post-infection with ova^{+} *Citrobacter*. **(H-K)** *Ifngr1*$^{fl/fl}$, *Ifngr1*$^{fl/fl}$ *Vil*^{CreERT2,} and *Ifngr1*$^{fl/fl}$ *Vil*^{CreERT2} *R26*$^{LSL\,Irf1}$ mice were infected with ova^{+} *Citrobacter rodentium* on day 0, injected with tamoxifen at days 3-6 post-infection, and analyzed on day 12 for CD4^{+} IE-T cells and **(I)** *Citrobacter* colonization in the colon (n = 5 per group). (**L**) *Ifngr1*$^{fl/fl}$ and *Ifngr1*$^{fl/fl}$ *Vil*^{Cre} mice were infected with *Citrobacter* and treated with isotype or anti-CD4 antibody every 2 days starting at day 7 analyzed for CD4^{+} T cells on day 12 p.i. (n = 8 per group). The horizontal bar represents the median, and each symbol represents an individual mouse. Data were analyzed by **(E** and **F)** Mann-Whitney U test (two-sided) or (**H-L**) Kruskal-Wallis test followed by Dunn's post-test.

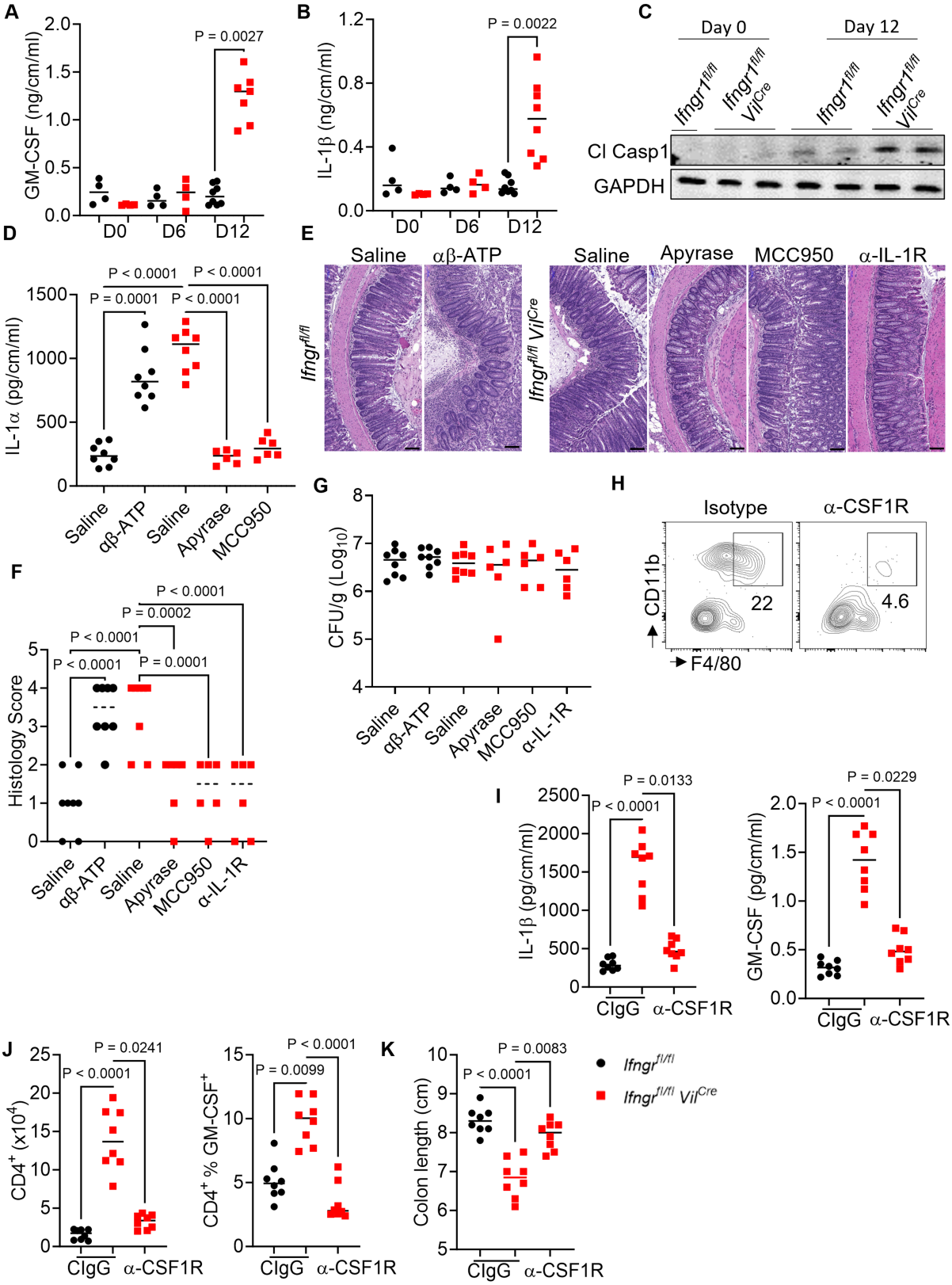

Extended Data Fig. 4 | Epithelial sensing of IFN-γ restrains NLRP3 inflammasome activation in macrophages. (A-K) *Ifngr1*$^{fl/fl}$ and *Ifngr1*$^{fl/fl}$ *Vil*^{Cre} mice were infected with *Citrobacter rodentium*. **(A** and **B)** Evaluation of indicated cytokines in colon explants (n = 4 for d0, d6 and n = 8 for d12, per group) and **(C)** immunoblotting for caspase-1 p10 in colon lysates, representative of two independent experiments. **(D)** Evaluation of IL-1α in colon explants, **(E-F)** Colon histology analyses and **(G)** *Citrobacter* colonization after isotype (n = 8), αβ-ATP (n = 8), apyrase (n = 6), MCC950 (n = 6) or anti-IL1R (n = 6) treatment. **(H-K)** *Ifngr1*$^{fl/fl}$ and *Ifngr1*$^{fl/fl}$ *Vil*^{Cre} mice were infected and given 500ug of anti-CSF1R or isotype control antibody on days 7, 9 and 11 p.i and sacrificed on day 12 p.i. (n = 8 per group). **(H)** Flow cytometric plot for colon macrophages from *Ifngr1*$^{fl/fl}$ *Vil*^{Cre} mice treated with anti-CSF1R or isotype control antibody. **(I)** Evaluation of indicated cytokines in colon explants. **(J)** Flow-cytometric analyses of CD4$^+$ IE-T cells and GM-CSF production from them and **(K)** colon length at day 12 p.i. Data were analyzed by Brown-Forsythe and Welch's ANOVA followed by Dunnett's post-test. Scale bar = 100 um.

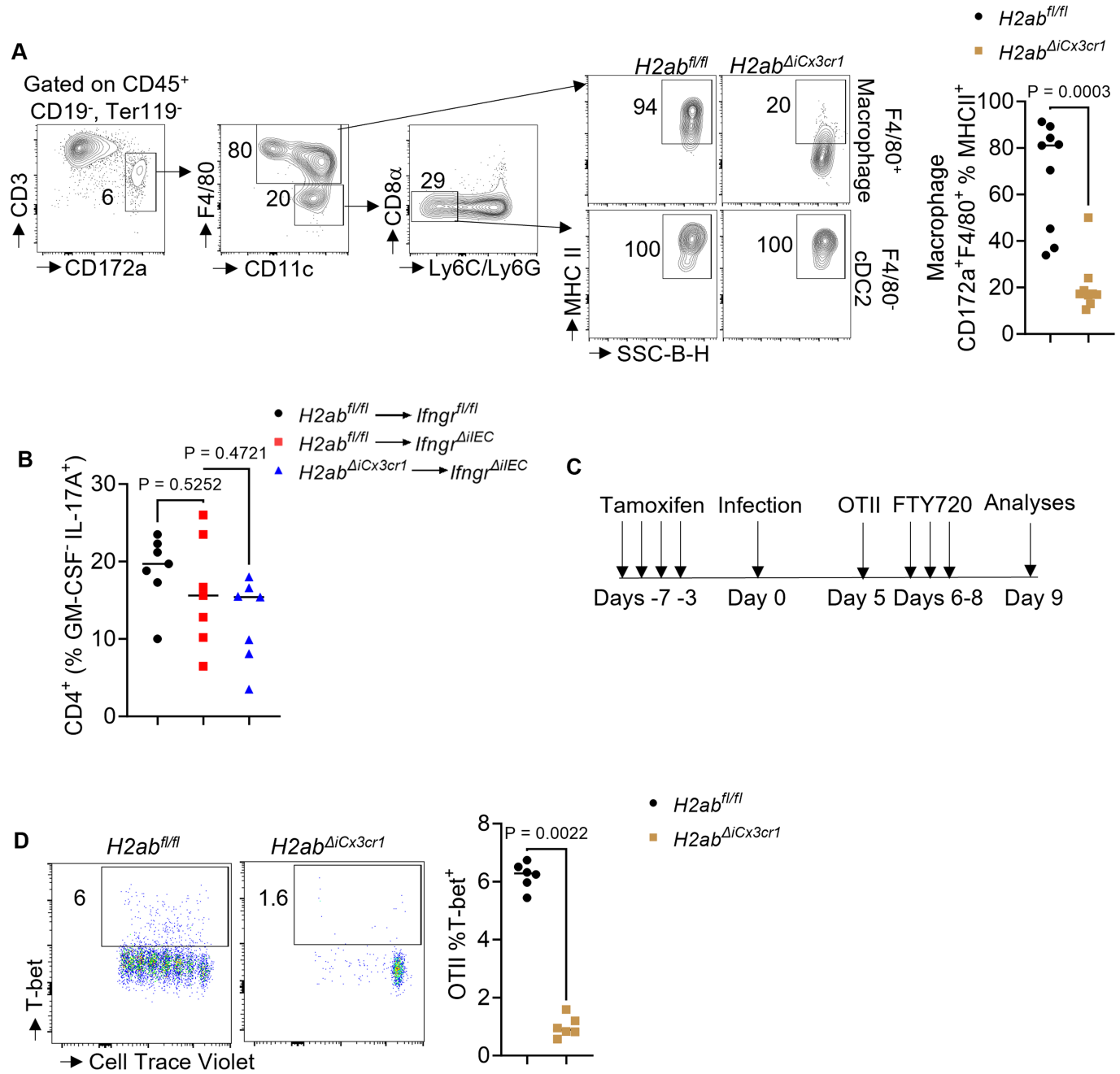

Extended Data Fig. 5 | Antigen presentation by CX3CR1+ APCs promote T_H1 immunity. *H2ab*$^{fl/fl}$ and *H2ab*$^{\Delta iCX3CR1}$ mice were infected with *Citrobacter*, injected with tamoxifen on days 3–6 and sacrificed on day 12 p.i. (**A**) Flow cytometric analyses of MHCII expression in CD172a$^+$ cells from the MLNs of *H2ab*$^{fl/fl}$ and *H2ab*$^{\Delta iCX3CR1}$ mice (n = 9 per group). (**B**) enumeration of GM-CSF$^-$ IL-17A$^+$ CD4$^+$ IE-T cells from the MLNs of *H2ab*$^{fl/fl}$»*Ifngr*$^{\Delta iIEC}$ and *H2ab*$^{\Delta iCX3CR1}$»*Ifngr*$^{\Delta iIEC}$ chimeric mice after treatments described in Fig. 3g at day 12 p.i. (n = 7 per group). (**C**) *H2ab*$^{fl/fl}$ and *H2ab*$^{\Delta iCX3RC1}$ mice were treated with tamoxifen for 4 consecutive days, followed by infection with *Citro*^{ova} 3 days after the last injection. Mice were injected with CTV-labelled 1×10^6 Rag-OTII cells on day 5 p.i., treated with 20ug of FTY720 i.p. on days 6-8 and sacrificed on day 9 (n = 6 per group). (**C**) Experimental scheme (**D**) OTII cells from MLNs were analyzed for T-bet induction. Data were analyzed by (**A** and **D**) by Mann-Whitney U test (two-sided) or (**B**) Kruskal-Wallis test followed by Dunn's post-test.

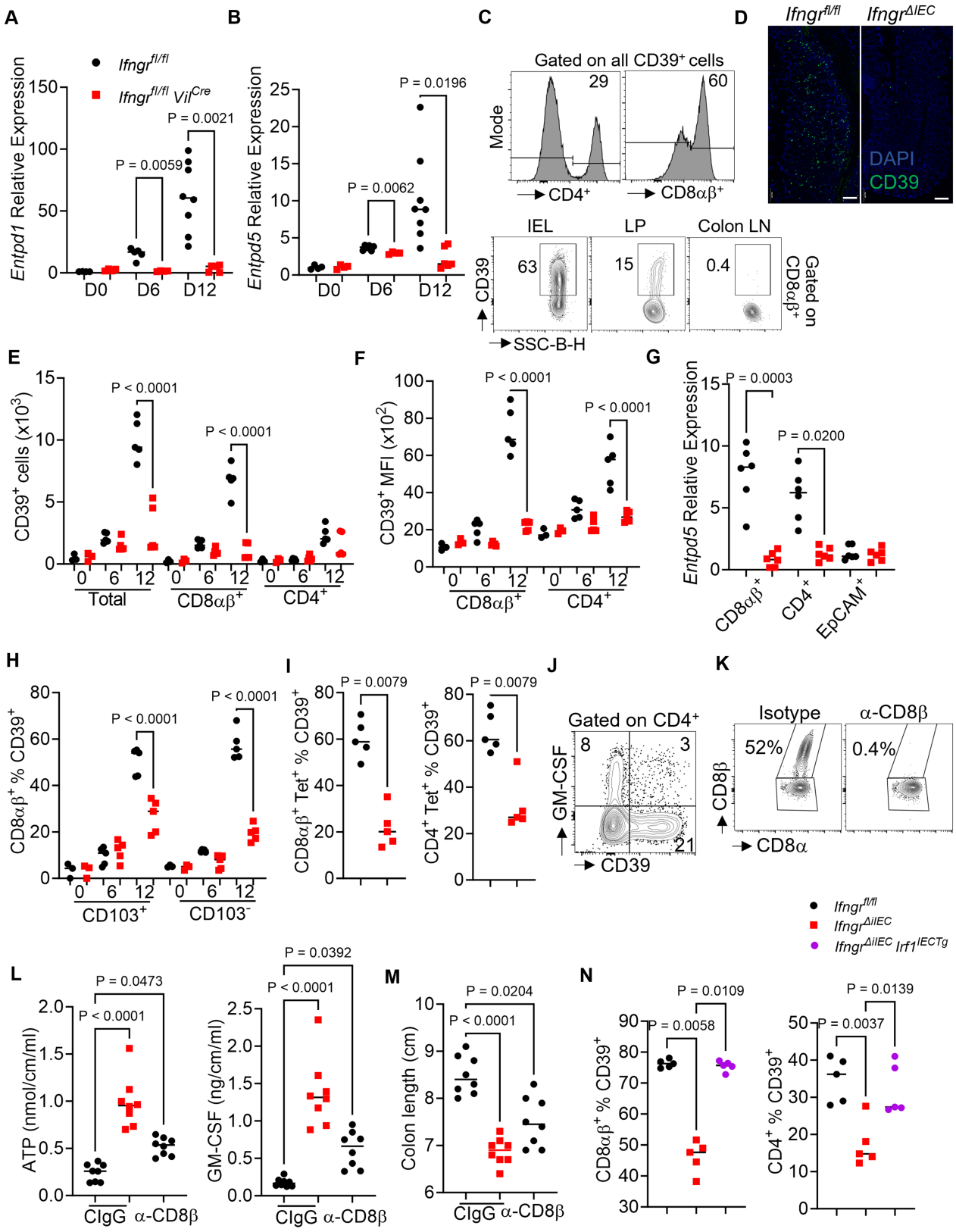

Extended Data Fig. 6 | See next page for caption.

Extended Data Fig. 6 | Epithelial sensing of IFN-γ promotes eATPase production from IE-T cells. (A-I) *Ifngr1*$^{fl/fl}$ and *Ifngr*$^{fl/fl}$ *Vil*^{Cre} mice were infected with *Citrobacter rodentium*. **(A** and **B)** RT-PCR analyses for indicated factors in colon epithelial tissue fraction (n = 4 for d0, d6 per group and n = 8 for *Ifngr1*$^{fl/fl}$ and n = 6 for *Ifngr1*$^{fl/fl}$ *Vil*^{Cre} for d12). **(C, E-I)** flow cytometric (n = 3 for d0, n = 5 for d6 and d12 per group) and (**D**) immunofluorescence evaluation of CD39 expression, representative of two independent experiments and **(G)** RT-PCR analyses of *Entpd5* expression from the purified IE-T cells and IECs (n = 6 per group). **(I)** *Ifngr1*$^{fl/fl}$ and *Ifngr1*$^{fl/fl}$ *Vil*^{Cre} mice were infected with ova^{+} *Citrobacter* and the ova-specific CD8αβ^{+} and CD4^{+} IE-T cells were evaluated for CD39 expression and **(J)** comparison of GM-CSF and CD39 producing CD4^{+} colonic IE-T cells in *Ifngr1*$^{fl/fl}$ mice at day 12 p.i. **(K-M)** *Ifngr1*$^{fl/fl}$ and *Ifngr1*$^{fl/fl}$ *Vil*^{Cre} mice were infected with *Citrobacter rodentium* and treated with 250ug isotype or CD8β-depleting antibodies every 2 days after the infection and sacrificed on day 12 p.i. (n = 8 per group). **(K)** FACS plot for CD8^{+} IE-T cells from mice given isotype or CD8β-depleting antibodies. **(L)** Colon explants were analyzed for indicated analytes and **(M)** colon length measurement. **(N)** *Ifngr1*$^{fl/fl}$, *Ifngr1*$^{fl/fl}$ *Vil*^{CreERT2} and *Ifngr1*$^{fl/fl}$ *Vil*^{CreERT2} *R26*^{LSLIrf1} mice were infected with *Citrobacter rodentium* on day 0, injected with tamoxifen at days 3–6 post-infection and analyzed on day 12 for CD39 expression from CD8αβ^{+} and CD4^{+} IE-T cells (n = 5 per group). The horizontal bar represents the median, and each symbol represents an individual mouse. Data were analyzed by **(A, B)** by Brown-Forsythe and Welch's ANOVA followed by Dunnett's post-test or **(E-I)** Mann-Whitney U test (two-sided) or (**L-N**) Kruskal-Wallis test followed by Dunn's post-test. Scale bar = 100 um.

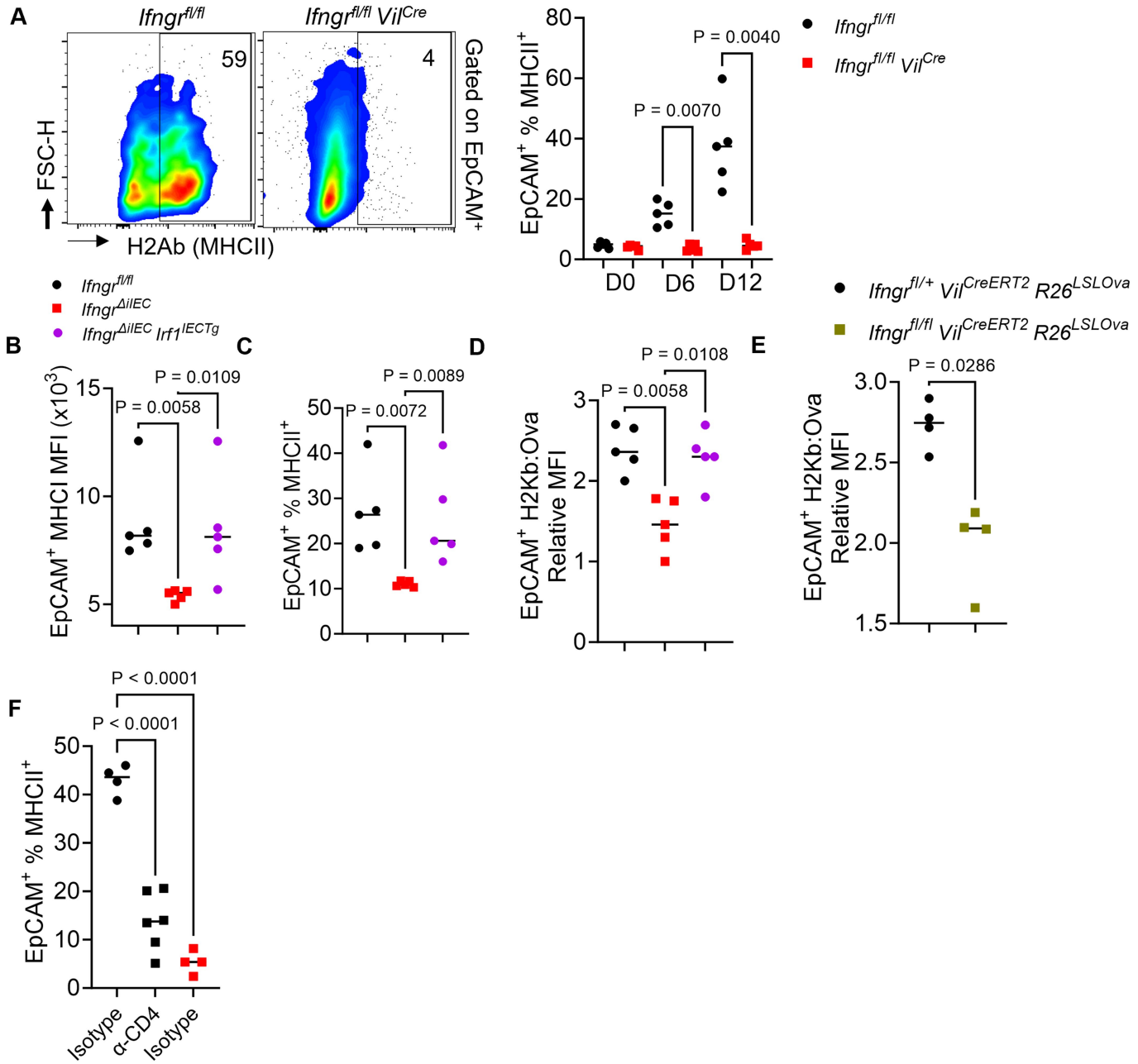

Extended Data Fig. 7 | Epithelial IFN-γ signaling controls antigen presentation by IECs. Flow cytometric enumeration of MHCII **(A** and **C)** or MHCI **(B)** or SIINFEKL-MHCI complex **(D-E)** on the surface of the colonic IECs after infection with *Citro*^{WT} **(A** and **E)** or *Citro*^{Ova} **(B-D)** at indicated day p.i. **(A)** or on day 12 p.i. (n = 5 per group). **(B-E).** Tamoxifen treatment was applied to induce the expression of the transgenes **(B-E)** at days 3-6 p.i. **(F)** *Ifngr1*$^{fl/fl}$ and *Ifngr1*$^{fl/fl}$ *Vil*^{Cre} mice were infected with *Citrobacter* and treated with anti-CD4 (n = 6) or isotype antibodies (n = 4) every 2 days starting at day 6 and sacrificed on day 12 p.i. The horizontal bar represents the median, and each symbol represents an individual mouse. Data were analyzed by **(A)** by ANOVA followed by Holm-Sidak post-test or **(B-D** and **F)** Kruskal-Wallis test followed by Dunn's post-test or **(E)** Mann-Whitney U test (two-sided).

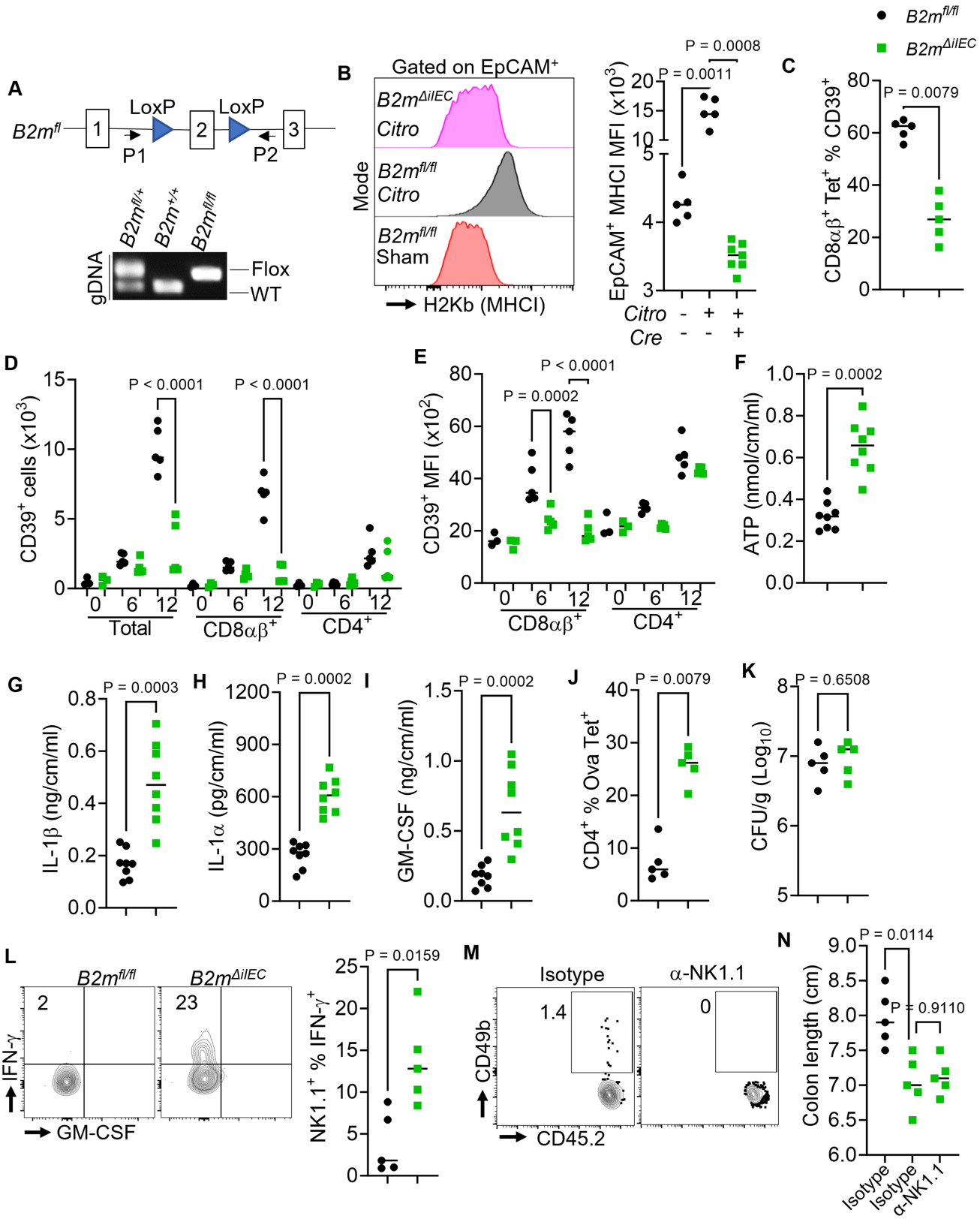

Extended Data Fig. 8 | See next page for caption.

Extended Data Fig. 8 | Antigen presentation via MHCI by IECs promotes eATPase production from CD8ab$^+$ IE-T cells. (A) Design and genotyping of *B2m*$^{fl/fl}$ mouse, representative of two independent lines. **(B-K)** *B2m*$^{fl/fl}$ and *B2m*$^{fl/fl}$*Vil*^{CreERT2} mice were infected with ova-expressing *Citrobacter* on day 0, treated with tamoxifen on days 3–6 and sacrificed on day 12. Colonic IECs on day 12 were analyzed for **(B)** MHCI expression (n = 5 for *B2m*$^{fl/fl}$ and n = 7 *B2m*$^{fl/fl}$ *Vil*^{CreERT2}) and (**C**) IE-T cells for CD39 expression (n = 5 per group) (**D-E**) (n = 3 for d0 and n = 5 for d6, d12 per group) by flow cytometry. **(F-I)** quantification of indicated analytes from colon explants (n = 8 per group) and **(J)** GM-CSF production from the ova-specific CD4$^+$ IE-T cells and **(K)** *Citrobacter* colonization in the colon at day 12 p.i. (n = 5 per group). (**L-N**) *B2m*$^{fl/fl}$ and *B2m*$^{fl/fl}$*Vil*^{CreERT2} mice were infected with ova-expressing *Citrobacter* on day 0, treated with tamoxifen on days 3–6, injected with anti-NK1.1 or isotype antibodies on days 2, 4, 6, 8 and 10 and sacrificed on day 12 (n = 5 per group). (**L**) IFN-γ production from NK1.1$^+$ TCRαβ$^-$ TCRγδ$^-$ cells (**M**) CD45$^+$CD49b$^+$ cells and (**N**) colon length at day 12. The horizontal bar represents the median, and each symbol represents an individual mouse. Data were analyzed by (**B, D, E** and **N**) ANOVA test followed by Sidak's post-test or **(C, F-L)** Kolmogorov-Smirnov test.

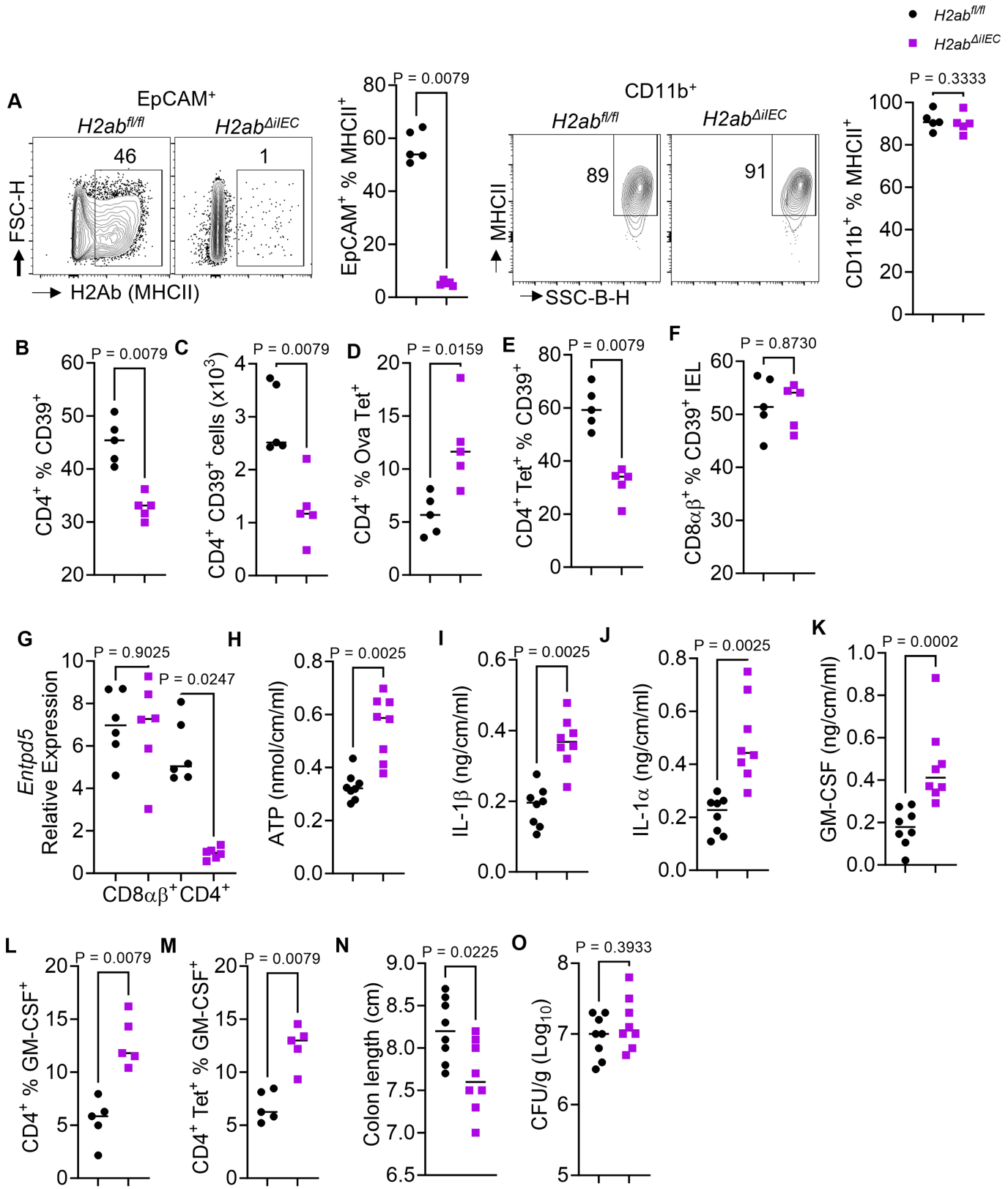

Extended Data Fig. 9 | Antigen presentation by IECs promotes eATPase production from CD4$^+$ IE-T cells. *H2ab*$^{fl/fl}$ and *H2ab*$^{fl/fl}$*Vil*^{CreERT2} mice were infected with ova-expressing *Citrobacter* on day 0, treated with tamoxifen on days 3-6, and sacrificed on day 12 (n = 5-8 per group). **(A)** Colonic IECs and myeloid cells were analyzed for MHCII expression on day 12 and (**C-F**) IE-T cells for CD39 expression by flow cytometry (n = 5 per group). (**G**) *Entpd5* expression by RT-PCR after purification (n = 6 per group). **(H-K)** quantification of indicated analytes from colon explants (n = 8 pe group). **(L-M)** GM-CSF production from the CD4$^+$ IE-T cells (n = 5 per group). **(N)** colon length and **(O)** *Citrobacter* colonization in the colon at day 12 p.i. (n = 8 per group). The horizontal bar represents the median, and each symbol represents an individual mouse. Data were analyzed by **(A-O)** Mann-Whitney U test (two-sided).

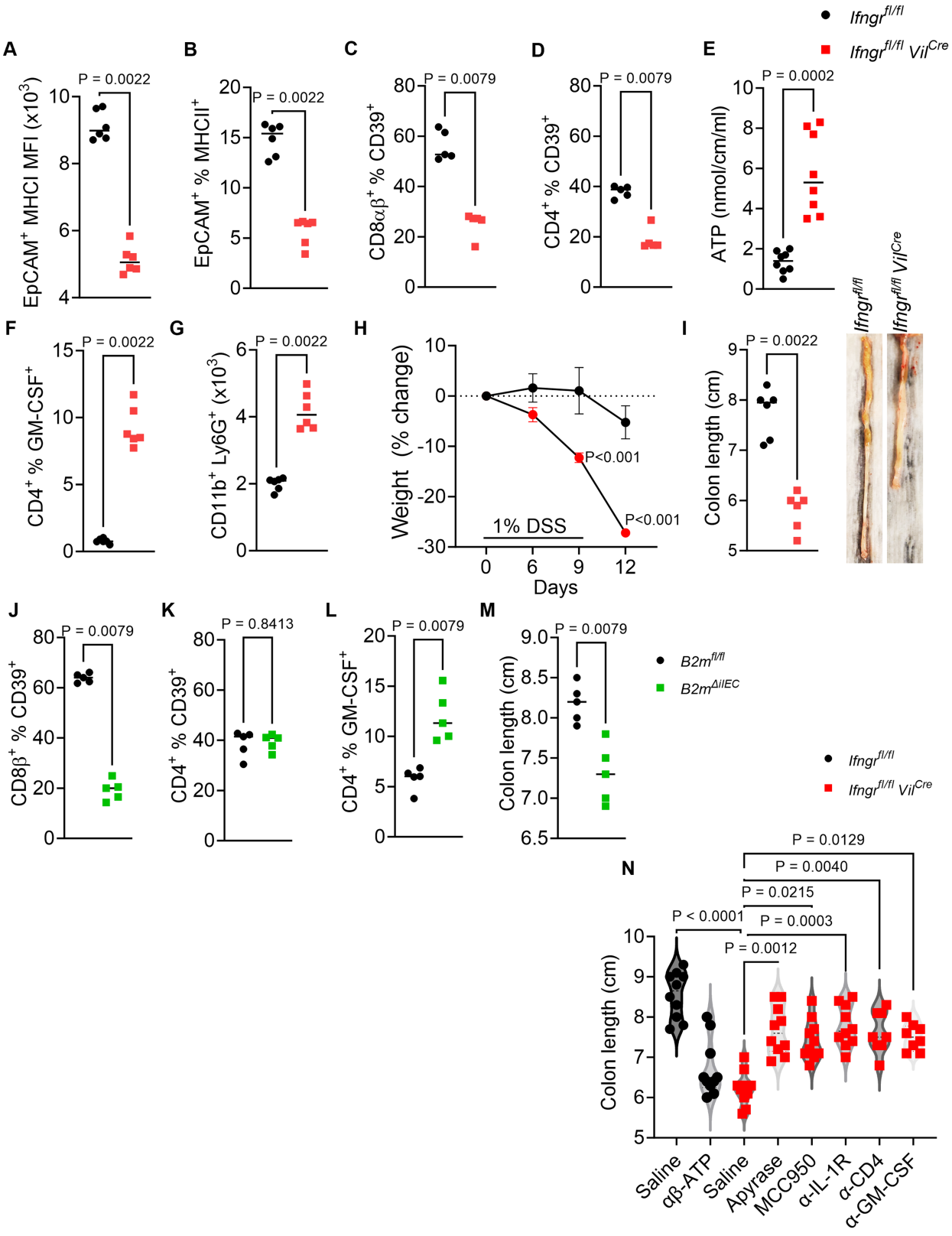

Extended Data Fig. 10 | See next page for caption.

Extended Data Fig. 10 | Antigen presentation by IECs restrains pathogenic CD4 T cells that promote chemical colitis. (**A-I**) *Ifngr1*$^{fl/fl}$ and *Ifngr1*$^{fl/fl}$*Vil*^{Cre} were treated with 1% DSS for 9 days followed by regular drinking water and sacrificed on day 12. **(A)** Expression of MHCI and **(B)** MHCII on the epithelial cell surface (n = 6 per group). Expression of CD39 on **(C)** CD8αβ^{+} and **(D)** CD4^{+} IE-T cells (n = 5 per group). (**E**) Quantification of ATP in the colon explants (n = 8 per group) and **(F)** production of GM-CSF from the CD4^{+} IE-T cells at day 12 (n = 5 per group). **(G)** Enumeration of neutrophils in the epithelium and (**H**) Bodyweight change and **(I)** colon length (n = 6 per group) and representative picture at day 12. **(J-M)** *B2m*$^{fl/fl}$ and *B2m*$^{fl/fl}$*Vil*^{CreERT2} mice (n = 5 per group) were treated with 1% DSS for 9 days followed by regular drinking water and sacrificed on day 12. Mice were also treated with tamoxifen on days 3-6. **(N)** Colon lengths from *Ifngr1*$^{fl/fl}$ and *Ifngr1*$^{fl/fl}$*Vil*^{Cre} mice treated isotype (n = 10), α-CD4 (n = 8), α-GM-CSF (n = 8), αβ-ATP (n = 10), apyrase (n = 10), MCC950 (n = 10) or α-IL1R (n = 10) during DSS administration and sacrificed on day 12. Each symbol represents an individual mouse, and the bar represents the median except for (**H**) where each dot indicated the mean and bar indicates the SEM. Data were analyzed by **(A-G, I-M)** Mann-Whitney U test (two-sided) or **(H)** ANOVA followed by Sidak post-test or **(N)** Kruskal-Wallis test followed by Dunn's post-test.

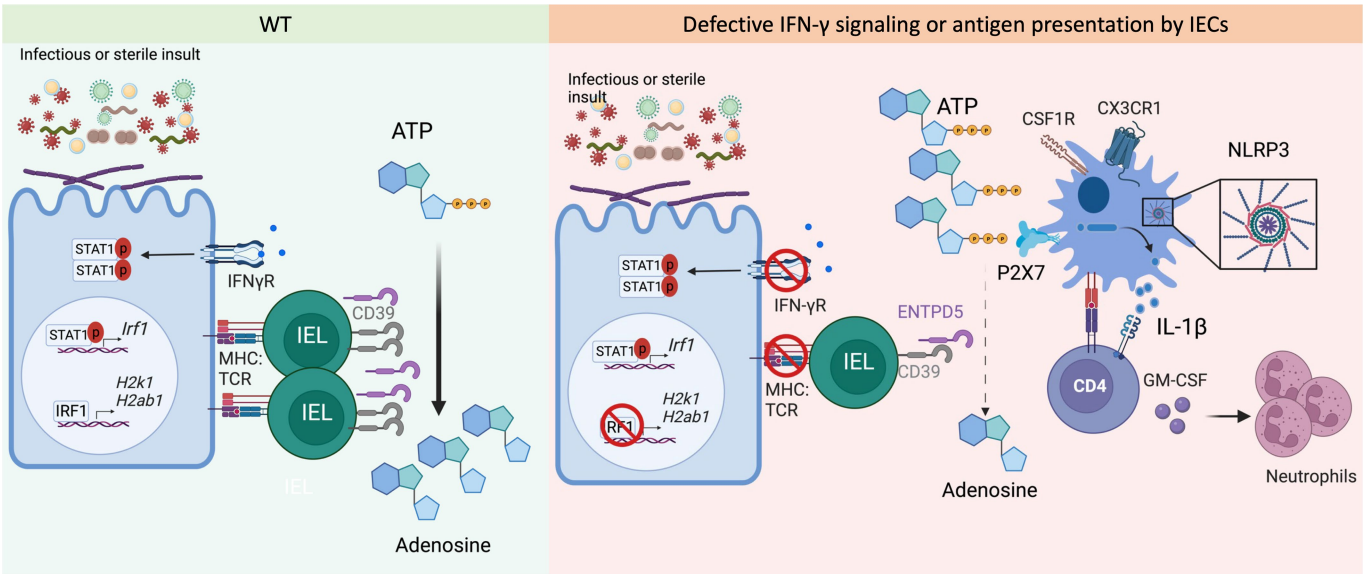

Extended Data Fig. 11 | Model. Upon sensing IFN-γ, colonic epithelial cells productively present pathogen-derived and self-antigens to the cognate intraepithelial T cells, critically situated at the epithelial barrier. Antigen presentation by the epithelial cells induces extracellular adenosine triphosphatase (ATPase) expression in the cognate intraepithelial T cells, which limits accumulation of extracellular ATP and resultant activation of the NLRP3 inflammasome in macrophages resident in the tissue. In contrast, macrophage antigen presentation alongside inflammasome-associated interleukin 1 alpha (IL-1α) and IL-1β production elicits pathogenic transformation of CD4-positive T cells into granulocyte-macrophage colony stimulating factor (GM-CSF)-producing T cells in vivo, promoting colitis and colorectal carcinogenesis. The figure was created using BioRender (https://biorender.com).

nature portfolio

Corresponding author(s): Drs. Bana Jabri and Ankit Malik

Last updated by author(s): Sep 12, 2023

Reporting Summary

Nature Portfolio wishes to improve the reproducibility of the work that we publish. This form provides structure for consistency and transparency in reporting. For further information on Nature Portfolio policies, see our Editorial Policies and the Editorial Policy Checklist.

Statistics

For all statistical analyses, confirm that the following items are present in the figure legend, table legend, main text, or Methods section.

n/a	Confirmed	
☐	☒	The exact sample size (*n*) for each experimental group/condition, given as a discrete number and unit of measurement
☐	☒	A statement on whether measurements were taken from distinct samples or whether the same sample was measured repeatedly
☐	☒	The statistical test(s) used AND whether they are one- or two-sided *Only common tests should be described solely by name; describe more complex techniques in the Methods section.*
☐	☒	A description of all covariates tested
☐	☒	A description of any assumptions or corrections, such as tests of normality and adjustment for multiple comparisons
☐	☒	A full description of the statistical parameters including central tendency (e.g. means) or other basic estimates (e.g. regression coefficient) AND variation (e.g. standard deviation) or associated estimates of uncertainty (e.g. confidence intervals)
☐	☒	For null hypothesis testing, the test statistic (e.g. *F*, *t*, *r*) with confidence intervals, effect sizes, degrees of freedom and *P* value noted *Give P values as exact values whenever suitable.*
☒	☐	For Bayesian analysis, information on the choice of priors and Markov chain Monte Carlo settings
☐	☒	For hierarchical and complex designs, identification of the appropriate level for tests and full reporting of outcomes
☐	☒	Estimates of effect sizes (e.g. Cohen's *d*, Pearson's *r*), indicating how they were calculated

Our web collection on statistics for biologists contains articles on many of the points above.

Software and code

Policy information about availability of computer code

Data collection	SpectroFlo, FACS Diva v8.0
Data analysis	FlowJo v10

For manuscripts utilizing custom algorithms or software that are central to the research but not yet described in published literature, software must be made available to editors and reviewers. We strongly encourage code deposition in a community repository (e.g. GitHub). See the Nature Portfolio guidelines for submitting code & software for further information.

Data

Policy information about availability of data

All manuscripts must include a data availability statement. This statement should provide the following information, where applicable:

- Accession codes, unique identifiers, or web links for publicly available datasets
- A description of any restrictions on data availability
- For clinical datasets or third party data, please ensure that the statement adheres to our policy

The datasets generated during the current study are available as supplementary files.

Human research participants

Policy information about studies involving human research participants and Sex and Gender in Research.

Reporting on sex and gender	N/A
Population characteristics	N/A
Recruitment	N/A
Ethics oversight	N/A

Note that full information on the approval of the study protocol must also be provided in the manuscript.

Field-specific reporting

Please select the one below that is the best fit for your research. If you are not sure, read the appropriate sections before making your selection.

☒ Life sciences ☐ Behavioural & social sciences ☐ Ecological, evolutionary & environmental sciences

For a reference copy of the document with all sections, see nature.com/documents/nr-reporting-summary-flat.pdf

Life sciences study design

All studies must disclose on these points even when the disclosure is negative.

Sample size	The majority of experiments were repeated at least two times to obtain data for indicated statistical analyses. Mice were allocated to experimental groups on the basis of their genotype and randomized within the given age-matched group. Given that our mice were inbred and matched for age, we always assumed similar variance between the different experimental group. We did not perform an a priori sample size estimation but always used as many mice per group as possible in an attempt to minimize type I and type II errors. There is no human data in the manuscript.
Data exclusions	There were no data exclusions.
Replication	All attempts at replication were successful and repeated twice.
Randomization	Mice were allocated to experimental groups on the basis of their genotype and randomized within given sex- and age-matched groups.
Blinding	Investigators were not blinded during experiments and outcome assessments, except for determination of histology as genotype information is required to setup and execute these experiments by the authors.

Reporting for specific materials, systems and methods

We require information from authors about some types of materials, experimental systems and methods used in many studies. Here, indicate whether each material, system or method listed is relevant to your study. If you are not sure if a list item applies to your research, read the appropriate section before selecting a response.

Materials & experimental systems

n/a	Involved in the study
☐	☒ Antibodies
☐	☒ Eukaryotic cell lines
☒	☐ Palaeontology and archaeology
☐	☒ Animals and other organisms
☒	☐ Clinical data
☒	☐ Dual use research of concern

Methods

n/a	Involved in the study
☒	☐ ChIP-seq
☐	☒ Flow cytometry
☒	☐ MRI-based neuroimaging

Antibodies

Antibodies used	CD45 Pac Blue (30-F11) Biolegend Cat#103126 TCRgd FITC (eBioGL3) Thermo Fisher Cat#11-5711-82 CD4 BV785 (GK1.5) Biolegend Cat#100453

CD4 BV605 (GK1.5) Biolegend Cat#100451
CD8β BUV395 (H35-17.2) BD Cat#740278
CD8α PerCp/Cy5.5 (53-6.7) BD Cat#551162
NK1.1 PE-CF594 (PK136) BD Cat#562864
TCRβ BUV737 (H57-597) BD Cat#612821
TCRβ BV711 (H57-597) BD Cat#563135
CD3ε BUV737 (145-2C11) BD Cat#612771
IFNγ APC (XMG1.2) BD Cat#554413
IL10 PEcy7 (JES5-16E3) Biolegend Cat#505026
IL17a PE (ebio17B7) Thermo Fisher Cat#12-7177-81
CD45.2 BUV395 (104) BD Cat#553772
RORγt BV786 (Q31-37) BD Cat#564723
FOXP3 eflour450 (FJK-16s) Thermo Fisher Cat#48-5773-82
FOXP3 FITC (FJK-16s) Thermo Fisher Cat#11-5773-82
Tbet PE (4B10) Biolegend Cat#644810
CD44 PE-CY7 (IM7) Biolegend Cat#103030
CD62L PE (MEL-14) Biolegend Cat#104408
Epcam PerCp/Cy5.5 (G8.8) Biolegend Cat#118220
CD19 FITC (1D3/CD19) Biolegend Cat#152404
NK1.1 BV605 (PK136) Biolegend Cat#108753
CD11C BV605 (N418) Biolegend Cat#117334
TER119 BV605 (TER-119) Biolegend Cat#116239
F4/80 BV605 (BM8) Biolegend Cat#123133
CD3ε BV605 (145-2C11) Biolegend Cat#100351
Ly6G BV605 (1A8) Biolegend Cat#127639
CD39 SB436 (24DMS1) Invitrogen Cat#62-0391-82
GM-CSF PE-CF594 (MP1-22E9) BioLegend Cat#505422
CD8b (53-5.8) Bio-X-Cell Cat# BE0223
GM-CSF (MP1-22E9) Bio-X-Cell Cat# BE0259
CD4 (YTS 177) Bio-X-Cell Cat# BP0003-3
IL-1R (CD121a) Bio-X-Cell Catalog #BE0256
IRDye® 680RD Goat anti-Rabbit IgG Secondary Antibody (LI-COR)

Validation

All antibodies are available commercially and were validated by manufacturers and in previous publications.

Eukaryotic cell lines

Policy information about cell lines and Sex and Gender in Research

Cell line source(s)	B16F10, ATCC
Authentication	Not authenticated
Mycoplasma contamination	Cell lines were not tested for mycoplasma contamination as they came with a contamination-free certification.
Commonly misidentified lines (See ICLAC register)	No commonly misidentified lines were used in this study

Animals and other research organisms

Policy information about studies involving animals; ARRIVE guidelines recommended for reporting animal research, and Sex and Gender in Research

Laboratory animals	Mice used in these studies are on the C57BL/6 background. Mice were maintained under specific pathogen-free conditions at the University of Chicago. Mice were used at 7-8 weeks of age.
Wild animals	No wild animals were used in this study
Reporting on sex	Similar numbers of male and female mice were used in all experiments.
Field-collected samples	No field-collected samples were utilized in this study
Ethics oversight	All experiments were performed in accordance with the Institutional Biosafety Committee and the Institutional Care and Use Committee of the University of Chicago.

Note that full information on the approval of the study protocol must also be provided in the manuscript.

Flow Cytometry

Plots

Confirm that:

☒ The axis labels state the marker and fluorochrome used (e.g. CD4-FITC).

☒ The axis scales are clearly visible. Include numbers along axes only for bottom left plot of group (a 'group' is an analysis of identical markers).

☒ All plots are contour plots with outliers or pseudocolor plots.

☒ A numerical value for number of cells or percentage (with statistics) is provided.

Methodology

Sample preparation	Single cells suspension were obtained from the gut epithelium, mesenteric lymph nodes, and blood. Intestinal epithelial cells were isolated by incubating gut fragments at 37C under agitation in EDTA containing calcium-free RPMI medium. A cell purification step using a 40% Percoll was used to enrich lymphocyte cell populations for flow cytometry analysis. Mesenteric lymph nodes were dissected, and made into a single cell suspension by mechanical disruption and passed through a 70µm nylon cell strainer. After collection of peripheral blood, erylysis was performed using the BD FACs lysing solution.
Instrument	Flow Cytometry analysis was perfomed on Cytek Aurora
Software	FACsDIVA software v10 (BD Biosciences) or SpectroFlo (Cyte4k Biosciences) was used to collect flow cytometry data and FlowJo software v10 (Treestar) was used to analyze them.
Cell population abundance	Many different types of cells were analyzed in this study, whose abundance varies with strain, genotype and treatment conditions as described in the main text and figures.
Gating strategy	All samples are FSC-A and SSC-A gated, followed by Live/Dead gating to select viable cells. Subsequent relevant gating was conducted as shown in figures and described in figure legends (Extended Figure 2A, Extended Figure 5A).

☒ Tick this box to confirm that a figure exemplifying the gating strategy is provided in the Supplementary Information.